J. Meas. Sci. Instrum., 2024, 15(4): 518-531.
DOI: 10.62756/jmsi.1674-8042.2024052
http://jmsi.publish.founderss.cn
jmsi@nuc.edu.cn

ICPS multi-target constrained comprehensive security control based on DoS attacks energy grading detection and compensation

HAN Yinlong[1], HAN Xiaowu[2*]

1. School of New Energy Engineering, Jiuquan Vocational Technical College, Jiuquan 735000, China;
2. School of Intelligent Manufacturing and Control Technology, Xi'an Mingde Institute of Technology, Xi'an 710000, China

***Corresponding author:** HAN Xiaowu (hanxw362@163.com)

Received: February 10, 2023 **Revised:** April 21, 2023 **Accepted:** May 15, 2023

Abstract: Aiming at the industry cyber-physical system (ICPS) where Denial-of-Service (DoS) attacks and actuator failure coexist, the integrated security control problem of ICPS under multi-objective constraints was studied. First, from the perspective of the defender, according to the differential impact of the system under DoS attacks of different energies, the DoS attacks energy grading detection standard was formulated, and the ICPS comprehensive security control framework was constructed. Secondly, a security transmission strategy based on event triggering was designed. Under the DoS attack energy classification detection mechanism, for large-energy attacks, the method based on time series analysis was considered to predict and compensate for lost data. Therefore, on the basis of passive and elastic response to small energy attacks, the active defense capability against DoS attacks was increased. Then by introducing the cone-complement linearization algorithm, the calculation methods of the state and fault estimation observer and the integrated safety controller were deduced, the goal of DoS attack active and passive hybrid intrusion tolerance and actuator failure active fault tolerance were realized. Finally, a simulation example of a four-capacity water tank system was given to verify the validity of the obtained conclusions.

Key words: industry cyber-physical system (ICPS); Denial-of-Service (DoS) attacks energy grading detection; security event triggering mechanism; time series analysis methods; cone complementary linearization

0 Introduction

New changes are constantly taking place in the field of industrial systems. Through the adoption of emerging internet-based concepts, technologies, tools, and methods, a new generation of industrial cyber-physical systems (ICPS) has emerged[1]. With the penetration of digitalization, networking, and intelligence in industrial systems, new vulnerabilities have emerged in ICPS while the interconnectivity has increased. This change has made ICPS security issues more and more prominent[2].

Network security plays an important role in the successful communication of system information. In practical applications, the transmission of information through communication networks may be subject to malicious attacks. There are more and more types of network attacks, such as Denial-of-Service (DoS) attacks[3], false data injection (FDI) attacks[4], replay attacks[5], malicious sensor node attacks[6], etc. Therefore, it is of great significance to study the security control design under network attack. DoS attacks are the easiest network attack to implement, and the attacker does not need to obtain prior knowledge of the system, so it is more common in industrial system[7,8]. Its purpose is to prevent the transmission of communication information in the system, which may lead to system performance degradation or even instability. Therefore, the issue of security control under DoS attacks has attracted extensive attention. The elastic control under DoS attacks was studied[9,10]. The optimal DoS attacks scheduling analysis and energy management have been studied[11,12]. And the predictive control based on event triggering under DoS attacks was also considered[13].

At the physical layer, actuators are also highly prone to failure in harsh industrial environments. It is well known that the fault-tolerant control (FTC) method can effectively compensate for the failure of the actuator and ensure the reliability and safety of the dynamic system[14-16]. Some effective linear-matrix collaborative FTC design methods were proposed[17,18]. However, in some practical systems, most of them are nonlinear, so it is very important to study the FTC of nonlinear

systems. The FTC problem of nonlinear multi-agent systems with switch topologies was solved[19]. However, the above achievements mainly focus on the security control method under the influence of actuator failure or network attack, and the research on the security control problem affected by the coupling of DoS attacks and actuator failure is seldom considered.

ICPS is a new generation of industrial engineering system, so it is necessary to consider the integrated security control of information security and physical security. In recent years, scholars have also made some achievements in the research of comprehensive security control. The adaptive event-triggered security control problem of a random nonlinear multi-agent system was studied under a class of DoS attacks and actuator failures, and a new fault-tolerant/intrusion-tolerant control method was proposed[20]. Passive event-triggered fault-tolerant control of actuator failure in networked control nonlinear systems was studied under DoS attacks, and a new periodic event-triggered sampling method was adopted[21]. The dual security control and communication collaborative design method for nonlinear cyber-physical systems was studied under the coexistence of actuator failure and DoS attacks[22]. However, these research results are obtained by using system flexibility to deal with DoS attacks intrusion, which is a passive intrusion-tolerant method in nature, and its tolerance to DoS attacks is limited.

Based on the above discussion and analysis, this study aimed to study the integrated security control method of ICPS under multi-objective constraints under the influence of limited energy DoS attacks and actuator fault coupling. The novelty and contributions of this paper are as follows.

1) From the perspective of the defender, according to the difference in the impact of DoS attacks with different energies, the impact of DoS attacks on the system was regarded as a special delay, the DoS energy classification standard was formulated, and the ICPS comprehensive security control framework was proposed.

2) A security transmission strategy based on event triggering was proposed, and a DoS attacks energy classification detection mechanism was designed. For large-energy DoS attacks, the method of sampling based on time series analysis was used to predict and compensate for the lost data, and to enhance the active defense capability of the system against DoS attacks.

3) Under the unified non-uniform transmission mechanism, considering the multi-objective constraints such as α-stability and γ suppression performance, a method of ICPS comprehensive security control and communication collaborative design under DoS attacks was given. And through the cone-complement linearization algorithm, the nonlinear problem in the design of the observer and the controller was transformed into a nonlinear programming problem constrained by a set of linear matrix inequalities.

1 System description

1.1 ICPS security control architecture under DoS energy classification

For the consideration of DoS attacks energy classification detection and intrusion tolerance strategy, Fig. 1 shows the ICPS integrated security control architecture. The main components of the system are the controlled object, intelligent sensing unit, control unit, and execution unit.

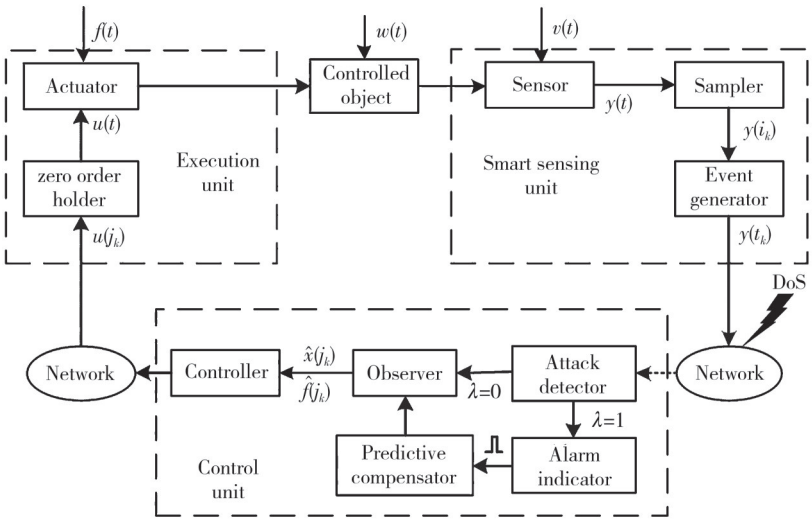

Fig. 1 ICPS integrated security control architecture

The limited energy DoS attacks acting on the sensor side network interrupt the information transmission by hindering normal communication, thus degrading the system performance or even destabilizing it.

In the intelligent sensing unit, the sensor is responsible for data measurement, and the sampler and event generator is responsible for data sampling and filtering. Reducing the frequency of data transmission can improve the system's tolerance to DoS attacks and reduce the communication burden.

In the control unit, the attack detector is responsible for DoS attacks energy classification detection and the alarm indicator is used for high-energy DoS attacks indication, and a pulse signal is sent to trigger the predictive compensator to predict and compensate for the lost data. Based on the data successfully transmitted or predicted and compensated, the observer estimates the state quantity and fault quantity, and the controller completes the corresponding control quantity calculation and finally transmits it to the execution unit through the network on the execution side.

In the execution unit, the zero-order holder is responsible for maintaining the non-uniform period of the control variable and then transmitting it to the actuator to acts on the controlled object.

1.2 Data timing analysis under non-uniform transmission

In order to actively defend against the DoS attacks on sensors, this section proposes an event-based security transmission strategy. The timing relationship of data transmission under finite energy DoS attacks is shown in Fig.2.

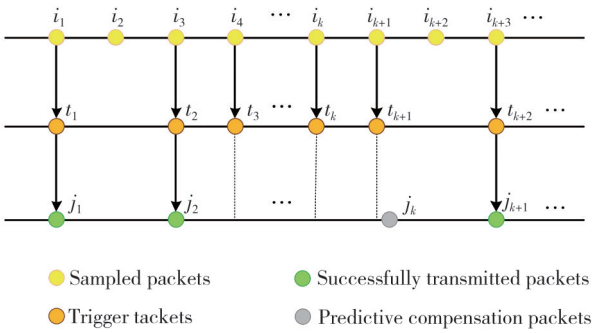

Fig. 2 Data update sequence diagram under non-uniform transmission

In Fig. 2, $i_k(k=1,2,\cdots)$ indicates the sampling moment of the sampler, and the sampling period is h, $t_k(k=1,2,\cdots)$ indicates the event trigger time, $j_k(k=1,2,\cdots)$ indicates the moment of data transmission after successful transmission or predicted compensation. Considering the event-triggered communication scheme on the sensor side, once $y(t_k)$ is successfully transmitted, the next trigger instant will be determined by the event-triggered conditions.

$$t_{k+1}=t_k+\min\{r_k,\bar{h}\},$$
$$r_k=\min_r\{r|[\boldsymbol{y}(t_k+r)-\boldsymbol{y}(t_k)]^{\mathrm{T}}\boldsymbol{\Phi}[\boldsymbol{y}(t_k+r)-\boldsymbol{y}(t_k)]\geqslant\sigma\boldsymbol{y}^{\mathrm{T}}(t_k+r)\boldsymbol{\Phi}\boldsymbol{y}(t_k+r)\}, \tag{1}$$

where $\sigma\in[0,1]$ is a predefined parameter; $\boldsymbol{\Phi}$ is a positive definite symmetric matrix; if t_k is the triggering time of the current event, the next triggering time t_{k+1} satisfies two conditions.

1) If $r_k\leqslant\bar{h}$, then $t_{k+1}=t_k+r_k$;

2) If $r_k>\bar{h}$, the next event trigger moment is defined as $t_{k+1}=t_k+\bar{h}$, $\bar{h}$ indicates the maximum event trigger interval between two adjacent trigger moments t_k and t_{k+1}, that is $t_{k+1}-t_k\leqslant\bar{h}$.

Combined with the idea of hierarchical intrusion tolerance proposed in this paper, the system delay caused by small-energy DoS attacks is small, and it will not have a large negative impact on system performance, utilizing the elastic robustness of the system to time delay to cope with small-energy DoS attacks. The large-energy DoS attacks will increase the system delay and the system performance loss. Therefore, it is necessary to predict and compensate for some lost data. Finally, the time sequence of data successfully received by the front end of the observer is $j_k(k=1,2,\cdots)$.

From the aforementioned security event trigger strategy, it can be seen that the data filtered by the trigger conditions are transmitted in a non-uniform cycle, so this system is a typical non-uniform sampling data system, which can be transformed into time-delay for analysis by using the relatively mature time-delay system theory[23]. For the non-uniform transmission problem and the impact of small energy DoS attacks, the delay function can be defined as

$$\tau(t)=t-j_k,t\in[j_k,j_{k+1}), \tag{2}$$

and the delay function satisfies $h\leqslant\tau(t)<\bar{h}$.

1.3 Controlled object model description

It can be seen from the ICPS safety control framework in Fig. 1 that the system is a typical sampling data system. Consider the linear ICPS model with actuator failure

$$\begin{cases}\dot{\boldsymbol{x}}(t)=\boldsymbol{A}\boldsymbol{x}(t)+\boldsymbol{B}\boldsymbol{u}(t)+\boldsymbol{E}_f\boldsymbol{f}(t)+\boldsymbol{B}_w\boldsymbol{w}(t),\\ \boldsymbol{y}(i_k)=\boldsymbol{C}\boldsymbol{x}(i_k)+\boldsymbol{E}_v\boldsymbol{v}(i_k),\end{cases} \tag{3}$$

where $\boldsymbol{A},\boldsymbol{B},\boldsymbol{E}_f,\boldsymbol{B}_w,\boldsymbol{C},\boldsymbol{E}_v$ are known suitable dimension

matrices; $\boldsymbol{x}(t)\in\mathbf{R}^{n}$, $\boldsymbol{u}(t)\in\mathbf{R}^{n_u}$, $\boldsymbol{y}(i_k)\in\mathbf{R}^{m}$ represent the system state vector, control input vector, and system sampling output, respectively; $\boldsymbol{w}(t)\in\mathbf{R}^{n_w}$, $\boldsymbol{v}(i_k)\in\mathbf{R}^{n_v}$ represent the system disturbance and sensor measurement noise, respectively; $\boldsymbol{f}(t)\in\mathbf{R}^{n_f}$ represents the continuous time-varying fault of the actuator, and the derivative norm is bounded, that is, there is a constant f_1, and $\left\|\dot{\boldsymbol{f}}(t)\right\|\leqslant f_1$.

2 DoS attacks active and passive hybrid intrusion tolerance strategy

2.1 Design of DoS attacks hierarchical detection mechanism

Combining Figs.1 and 2, it can be seen that regardless of whether DoS attacks occur or not, the transmission interval of system measurement output data is $T=j_{k+1}-j_k$. Considering the data security transmission strategy and the improvement of control performance, the maximum security event trigger interval $\bar{h}$ is taken as the standard for distinguishing the energy of DoS attacks. If the data transmission interval $T\leqslant\bar{h}$, it is considered that the system has not suffered DoS attacks or suffered small-energy DoS attacks. If $T>\bar{h}$, then it is considered that the system has suffered large-energy DoS attacks. Based on the energy classification standard formulated above, whether large-energy DoS attacks occur is determined by the alarm factors λ, that is

$$\lambda=\begin{cases}0, & \text{other},\\ 1, & T>\beta\bar{h},\end{cases}\tag{4}$$

where $\beta\in(0,1)$is the safety factor. When $\lambda=1$, the data prediction compensation mechanism will be triggered.

2.2 Design of tolerance strategy for DoS attacks

Under the security event trigger mechanism, for small-energy DoS attacks, the data transmission delay is limited within the maximum security trigger interval $\bar{h}$, and the robustness of ICPS to delay is used to deal with it. For large-energy DoS attacks, the data transmission delay caused by them is greater than the maximum safe trigger interval $\bar{h}$. If large-energy DoS attacks are detected at time j_k, and $y(j_k)$ has been discarded at this time, it is necessary to predict and compensate for the lost data, that is, to carry out the active invasion.

The method based on time series analysis is considered to predict and compensate for the missing data, the autoregressive moving average mixed model ARMA (p,q) is used to predict the missing data. It is a mixed form of the autoregressive model (AR) and the moving average model (MA), so it is also called the autoregressive moving average mixed model. Its equation form is

$$\begin{aligned}\boldsymbol{y}_{pre}(j_k)=&\boldsymbol{c}+\boldsymbol{\phi}_1\boldsymbol{y}(j_{k-1})+\boldsymbol{\phi}_2\boldsymbol{y}(j_{k-2})+\cdots+\\&\boldsymbol{\phi}_p\boldsymbol{y}(j_{k-p})+\boldsymbol{e}_k-\theta_1\boldsymbol{e}_{k-1}-\theta_2\boldsymbol{e}_{k-2}-\cdots-\theta_q\boldsymbol{e}_{k-q},\end{aligned}\tag{5}$$

where $\boldsymbol{c}$ is a constant; $\boldsymbol{\phi}_1,\boldsymbol{\phi}_2,\cdots,\boldsymbol{\phi}_p$ is the coefficient of autoregressive model AR; p is the order of AR; $\theta_1,\theta_2,\cdots,\theta_q$ is the coefficient of moving average model MA; q is the order of MA; $\boldsymbol{e}_k$ is a white noise sequence with mean value 0 and variance σ^2.

Through the compensation method, the measurement data received by the front end of the final observer can be expressed by

$$\bar{\boldsymbol{y}}(j_k)=\begin{cases}\boldsymbol{y}(j_k), & \lambda=0,\\ \boldsymbol{y}_{\text{pre}}(j_k), & \lambda=1.\end{cases}\tag{6}$$

3 Design of multi-object constrained observer under DoS energy classification

Combining Eqs. (2) and (6), the fcontinuous time-varying delay output can be obtained by

$$\bar{\boldsymbol{y}}(t)=\begin{cases}\boldsymbol{y}(t-\tau(t)), & \lambda=0,\\ \boldsymbol{y}_{\text{pre}}(t-\tau(t)), & \lambda=1.\end{cases}\tag{7}$$

Construct the state and fault estimation observer, that is

$$\begin{cases}\dot{\hat{\boldsymbol{x}}}(t)=\boldsymbol{A}\hat{\boldsymbol{x}}(t)+\boldsymbol{B}\boldsymbol{u}(t)+\boldsymbol{E}_f\hat{\boldsymbol{f}}(t)-\boldsymbol{L}\left[\hat{\boldsymbol{y}}(t)-\bar{\boldsymbol{y}}(t)\right],\\ \hat{\boldsymbol{y}}(t)=\boldsymbol{C}\hat{\boldsymbol{x}}(t-\tau(t)),\\ \dot{\hat{\boldsymbol{f}}}(t)=-\boldsymbol{F}\left[\hat{\boldsymbol{y}}(t)-\bar{\boldsymbol{y}}(t)\right],\end{cases}\tag{8}$$

where $\hat{\boldsymbol{x}}(t)$ and $\hat{\boldsymbol{y}}(t)$ are system state estimation value and observer output value, respectively, $\hat{\boldsymbol{f}}(t)$ is fault estimation value; $\boldsymbol{L}$ and $\boldsymbol{F}$ are observer gain matrix and fault gain matrix, respectively.

Define $\begin{cases}\boldsymbol{e}_x(t)=\hat{\boldsymbol{x}}(t)-\boldsymbol{x}(t),\\ \boldsymbol{e}_y(t)=\hat{\boldsymbol{y}}(t)-\bar{\boldsymbol{y}}(t),\\ \boldsymbol{e}_f(t)=\hat{\boldsymbol{f}}(t)-\boldsymbol{f}(t),\end{cases}$ the error system can be obtained by

$$\begin{cases}\dot{\boldsymbol{e}}_x(t)=\dot{\hat{\boldsymbol{x}}}(t)-\dot{\boldsymbol{x}}(t)=\boldsymbol{A}\boldsymbol{e}_x(t)+\boldsymbol{E}_f\boldsymbol{e}_f(t)-\\ \qquad\boldsymbol{L}\boldsymbol{C}\boldsymbol{e}_x(t-\tau(t))+\boldsymbol{L}\boldsymbol{E}_v(t-\tau(t))-\boldsymbol{B}_w\boldsymbol{w}(t),\\ \boldsymbol{e}_y(t)=\boldsymbol{C}\boldsymbol{e}_x(t-\tau(t))-\boldsymbol{E}_v\boldsymbol{v}(t-\tau(t)).\end{cases}\tag{9}$$

The derivative of the fault estimation error with respect to time is given by

$$\dot{\boldsymbol{e}}_f(t)=-\boldsymbol{F}\boldsymbol{C}\boldsymbol{e}_x(t-\tau(t))+\boldsymbol{F}\boldsymbol{E}_v\boldsymbol{v}(t-\tau(t))-\dot{\boldsymbol{f}}(t). \tag{10}$$

Combining Eqs. (9) and (10), the augmented error system can be obtained by

$$\dot{\bar{\boldsymbol{e}}}(t)=\bar{\boldsymbol{A}}\bar{\boldsymbol{e}}(t)-\bar{\boldsymbol{L}}\bar{\boldsymbol{C}}\bar{\boldsymbol{e}}(t-\tau(t))-\bar{\boldsymbol{B}}_w\bar{\boldsymbol{w}}(t)+\bar{\boldsymbol{L}}\boldsymbol{E}_v\boldsymbol{v}(t-\tau(t)), \tag{11}$$

where $\bar{\boldsymbol{A}}=\begin{bmatrix}\boldsymbol{A} & \boldsymbol{E}_f\\ 0 & 0\end{bmatrix}$, $\bar{\boldsymbol{e}}(t)=\begin{bmatrix}\boldsymbol{e}_x(t)\\ \boldsymbol{e}_f(t)\end{bmatrix}$, $\bar{\boldsymbol{C}}=[\boldsymbol{C}\quad 0]$, $\bar{\boldsymbol{L}}=\begin{bmatrix}\boldsymbol{L}\\ \boldsymbol{F}\end{bmatrix}$, $\bar{\boldsymbol{B}}_w=\begin{bmatrix}\boldsymbol{B}_w & 0\\ 0 & \boldsymbol{I}\end{bmatrix}$, $\bar{\boldsymbol{w}}(t)=\begin{bmatrix}\boldsymbol{w}(t)\\ \dot{\boldsymbol{f}}(t)\end{bmatrix}$.

Theorem 1 Given a positive number a, if there exist $\alpha_1,\bar{h},\gamma_1$, positive definite symmetric matrices $\boldsymbol{P},\boldsymbol{Q},\boldsymbol{R},\boldsymbol{Z}$, and matrices $\boldsymbol{M},\boldsymbol{Y}$ of appropriate dimension satisfying linear matrix inequalities (12) and (13), then there are observer gain matrix $\boldsymbol{L}$ and fault gain matrix $\boldsymbol{F}$, for DoS attacks at different energy levels, the dynamic error system (11) can be asymptotically α-stable when there is no disturbance, and the performance index can be satisfied when there is disturbance.

$$\left\|\bar{\boldsymbol{e}}_{\alpha_1}(t)\right\|_2^2\leqslant\gamma_1^2\left(\left\|\bar{\boldsymbol{w}}_{\alpha_1}(t)\right\|_2^2+\sum_{k=0}^{+\infty}(j_{k+1}-j_k)\left\|\boldsymbol{v}_{\alpha_1}(j_k)\right\|_2^2\right),$$

$\boldsymbol{L}$ and $\boldsymbol{F}$ can be obtained from $\bar{\boldsymbol{L}}=\begin{bmatrix}\boldsymbol{L}\\ \boldsymbol{F}\end{bmatrix}$.

$$\begin{bmatrix}\boldsymbol{U}_{11} & \boldsymbol{U}_{12} & \boldsymbol{U}_{13} & \boldsymbol{U}_{14} & \boldsymbol{U}_{15} & \boldsymbol{M}^{\mathrm{T}} & \boldsymbol{U}_{17} & \boldsymbol{U}_{18}\\ * & \boldsymbol{U}_{22} & \boldsymbol{U}_{23} & \boldsymbol{U}_{24} & \boldsymbol{U}_{25} & \boldsymbol{M}^{\mathrm{T}} & 0 & 0\\ * & * & \boldsymbol{U}_{33} & \boldsymbol{U}_{34} & \boldsymbol{U}_{35} & \boldsymbol{M}^{\mathrm{T}} & 0 & 0\\ * & * & * & \boldsymbol{U}_{44} & \boldsymbol{U}_{45} & \boldsymbol{M}^{\mathrm{T}} & 0 & 0\\ * & * & * & * & \boldsymbol{U}_{55} & \boldsymbol{M}^{\mathrm{T}} & \boldsymbol{U}_{57} & \boldsymbol{U}_{58}\\ * & * & * & * & * & \boldsymbol{U}_{66} & 0 & 0\\ * & * & * & * & * & * & \boldsymbol{U}_{77} & 0\\ * & * & * & * & * & * & * & \boldsymbol{U}_{88}\end{bmatrix}<0, \tag{12}$$

$$\begin{bmatrix}\boldsymbol{V}_{11} & \boldsymbol{V}_{12} & \boldsymbol{V}_{13} & \boldsymbol{V}_{14} & \boldsymbol{V}_{15} & \boldsymbol{V}_{16} & \boldsymbol{V}_{17} & \boldsymbol{M}^{\mathrm{T}} & \boldsymbol{V}_{19} & \boldsymbol{V}_{110}\\ * & \boldsymbol{V}_{22} & \boldsymbol{V}_{23} & \boldsymbol{V}_{24} & \boldsymbol{V}_{25} & 0 & 0 & \boldsymbol{M}^{\mathrm{T}} & 0 & 0\\ * & * & \boldsymbol{V}_{33} & \boldsymbol{V}_{34} & \boldsymbol{V}_{35} & 0 & 0 & \boldsymbol{M}^{\mathrm{T}} & 0 & 0\\ * & * & * & \boldsymbol{V}_{44} & \boldsymbol{V}_{45} & 0 & 0 & \boldsymbol{M}^{\mathrm{T}} & 0 & 0\\ * & * & * & * & \boldsymbol{V}_{55} & 0 & 0 & \boldsymbol{M}^{\mathrm{T}} & \boldsymbol{V}_{59} & \boldsymbol{V}_{510}\\ * & * & * & * & * & \boldsymbol{V}_{66} & 0 & 0 & \boldsymbol{V}_{69} & \boldsymbol{V}_{610}\\ * & * & * & * & * & * & \boldsymbol{V}_{77} & 0 & \boldsymbol{V}_{79} & \boldsymbol{V}_{710}\\ * & * & * & * & * & * & * & \boldsymbol{V}_{88} & 0 & 0\\ * & * & * & * & * & * & * & * & \boldsymbol{V}_{99} & 0\\ * & * & * & * & * & * & * & * & * & \boldsymbol{V}_{1010}\end{bmatrix}<0, \tag{13}$$

where * is the transpose of a symmetric matrix, and

$\boldsymbol{U}_{11}=\boldsymbol{P}\bar{\boldsymbol{A}}+\bar{\boldsymbol{A}}^{\mathrm{T}}\boldsymbol{P}+\boldsymbol{Q}-\boldsymbol{R}+3\boldsymbol{M}+3\boldsymbol{M}^{\mathrm{T}}$,

$\boldsymbol{U}_{12}=3\boldsymbol{M}-\boldsymbol{M}^{\mathrm{T}}$, $\boldsymbol{U}_{13}=3\boldsymbol{M}-8\boldsymbol{M}^{\mathrm{T}}$,

$\boldsymbol{U}_{14}=3\boldsymbol{M}+12\boldsymbol{M}^{\mathrm{T}}$, $\boldsymbol{U}_{15}=-\boldsymbol{e}^{\alpha_1\tau(t)}\boldsymbol{Y}\bar{\boldsymbol{C}}+3\boldsymbol{M}$,

$\boldsymbol{U}_{17}=\bar{h}\bar{\boldsymbol{A}}^{\mathrm{T}}\boldsymbol{P}$, $\boldsymbol{U}_{18}=\sqrt{\bar{h}}\,\bar{\boldsymbol{A}}^{\mathrm{T}}\boldsymbol{P}$,

$\boldsymbol{U}_{22}=-\boldsymbol{Q}-\boldsymbol{M}-\boldsymbol{M}^{\mathrm{T}}$, $\boldsymbol{U}_{23}=-\boldsymbol{M}-8\boldsymbol{M}^{\mathrm{T}}$,

$\boldsymbol{U}_{24}=-\boldsymbol{M}+12\boldsymbol{M}^{\mathrm{T}}$, $\boldsymbol{U}_{25}=-\boldsymbol{M}$,

$\boldsymbol{U}_{33}=-8\boldsymbol{M}-8\boldsymbol{M}^{\mathrm{T}}$, $\boldsymbol{U}_{34}=-8\boldsymbol{M}+12\boldsymbol{M}^{\mathrm{T}}$,

$\boldsymbol{U}_{35}=-8\boldsymbol{M}$, $\boldsymbol{U}_{44}=12\boldsymbol{M}+12\boldsymbol{M}^{\mathrm{T}}$, $\boldsymbol{U}_{45}=12\boldsymbol{M}$,
$\boldsymbol{U}_{55}=\boldsymbol{R}$, $\boldsymbol{U}_{57}=-\bar{h}\boldsymbol{e}^{\alpha_1\tau(t)}(\boldsymbol{Y}\bar{\boldsymbol{C}})^{\mathrm{T}}$,

$\boldsymbol{U}_{58}=-\sqrt{\bar{h}}\,\boldsymbol{e}^{\alpha_1\tau(t)}(\boldsymbol{Y}\bar{\boldsymbol{C}})^{\mathrm{T}}$, $\boldsymbol{U}_{66}=\dfrac{1}{-9h}\boldsymbol{Z}^{-1}$,

$\boldsymbol{U}_{77}=-\boldsymbol{P}\boldsymbol{R}^{-1}\boldsymbol{P}$, $\boldsymbol{U}_{88}=-\boldsymbol{P}\boldsymbol{Z}^{-1}\boldsymbol{P}$,

$\boldsymbol{V}_{11}=\boldsymbol{P}\bar{\boldsymbol{A}}+\bar{\boldsymbol{A}}^{\mathrm{T}}\boldsymbol{P}+\boldsymbol{Q}-\boldsymbol{R}+3\boldsymbol{M}+3\boldsymbol{M}^{\mathrm{T}}+\boldsymbol{I}$,

$\boldsymbol{V}_{12}=3\boldsymbol{M}-\boldsymbol{M}^{\mathrm{T}}$, $\boldsymbol{V}_{13}=3\boldsymbol{M}-8\boldsymbol{M}^{\mathrm{T}}$,

$\boldsymbol{V}_{14}=3\boldsymbol{M}+12\boldsymbol{M}^{\mathrm{T}}$, $\boldsymbol{V}_{15}=-\boldsymbol{e}^{\alpha_1\tau(t)}\boldsymbol{Y}\bar{\boldsymbol{C}}+3\boldsymbol{M}$,

$\boldsymbol{V}_{16}=\boldsymbol{e}^{\alpha_1\tau(t)}\boldsymbol{P}\bar{\boldsymbol{L}}\boldsymbol{E}_v$, $\boldsymbol{V}_{17}=-\boldsymbol{P}\bar{\boldsymbol{B}}_w$, $\boldsymbol{V}_{19}=\bar{h}\bar{\boldsymbol{A}}^{\mathrm{T}}\boldsymbol{P}$,

$\boldsymbol{V}_{110}=\sqrt{\bar{h}}\,\bar{\boldsymbol{A}}^{\mathrm{T}}\boldsymbol{P}$, $\boldsymbol{V}_{22}=-\boldsymbol{Q}-\boldsymbol{M}-\boldsymbol{M}^{\mathrm{T}}$,

$\boldsymbol{V}_{23}=-\boldsymbol{M}-8\boldsymbol{M}^{\mathrm{T}}$, $\boldsymbol{V}_{24}=-\boldsymbol{M}+12\boldsymbol{M}^{\mathrm{T}}$,

$\boldsymbol{V}_{25}=-\boldsymbol{M}$, $\boldsymbol{V}_{33}=-8\boldsymbol{M}-8\boldsymbol{M}^{\mathrm{T}}$,

$\boldsymbol{V}_{34}=-8\boldsymbol{M}+12\boldsymbol{M}^{\mathrm{T}}$, $\boldsymbol{V}_{35}=-8\boldsymbol{M}$,

$\boldsymbol{V}_{44}=12\boldsymbol{M}+12\boldsymbol{M}^{\mathrm{T}}$, $\boldsymbol{V}_{45}=12\boldsymbol{M}$, $\boldsymbol{V}_{55}=\boldsymbol{R}$,

$\boldsymbol{V}_{59}=-\bar{h}\boldsymbol{e}^{\alpha_1\tau(t)}(\boldsymbol{Y}\bar{\boldsymbol{C}})^{\mathrm{T}}$, $\boldsymbol{V}_{510}=-\sqrt{\bar{h}}\,\boldsymbol{e}^{\alpha_1\tau(t)}(\boldsymbol{Y}\bar{\boldsymbol{C}})^{\mathrm{T}}$,

$\boldsymbol{V}_{66}=-\gamma_1^2\boldsymbol{I}$, $\boldsymbol{V}_{69}=-\bar{h}\boldsymbol{e}^{\alpha_1\tau(t)}(\boldsymbol{Y}\boldsymbol{E}_v)^{\mathrm{T}}$,

$\boldsymbol{V}_{610}=-\sqrt{\bar{h}}\,\boldsymbol{e}^{\alpha_1\tau(t)}(\boldsymbol{Y}\boldsymbol{E}_v)^{\mathrm{T}}$, $\boldsymbol{V}_{77}=-\gamma_1^2\boldsymbol{I}$,

$\boldsymbol{V}_{79}=\bar{h}\bar{\boldsymbol{B}}_w^{\mathrm{T}}\boldsymbol{P}$, $\boldsymbol{V}_{79}=-\sqrt{\bar{h}}\,\bar{\boldsymbol{B}}_w^{\mathrm{T}}\boldsymbol{P}$, $\boldsymbol{U}_{88}=\dfrac{1}{-9h}\boldsymbol{Z}^{-1}$,

$\boldsymbol{U}_{99}=-\boldsymbol{P}\boldsymbol{R}^{-1}\boldsymbol{P}$, $\boldsymbol{U}_{1010}=-\boldsymbol{P}\boldsymbol{Z}^{-1}\boldsymbol{P}$.

Proof: introducing the state transition $\boldsymbol{x}(t)=\boldsymbol{e}^{-\alpha_1 t}\boldsymbol{\zeta}(t)$, Eqs. (3) and (7) can be transformed as Eqs. (14) and (15)

$$\begin{cases}\dot{\boldsymbol{\zeta}}(t)=\tilde{\boldsymbol{A}}\boldsymbol{\zeta}(t)+\boldsymbol{B}\boldsymbol{u}_{\alpha_1}(t)+\boldsymbol{E}_f\boldsymbol{f}_{\alpha_1}(t)+\boldsymbol{B}_w\boldsymbol{w}_{\alpha_1}(t),\\ \boldsymbol{y}_{\alpha_1}(t)=\boldsymbol{C}\boldsymbol{\zeta}(t-\tau(t))+\boldsymbol{E}_v\boldsymbol{v}_{\alpha_1}(t-\tau(t)),\end{cases} \tag{14}$$

where $\tilde{\boldsymbol{A}}=\boldsymbol{A}+\alpha_1\boldsymbol{I}$, $\boldsymbol{u}_{\alpha_1}(t)=\boldsymbol{e}^{\alpha_1 t}\boldsymbol{u}(t)$, $\boldsymbol{f}_{\alpha_1}(t)=\boldsymbol{e}^{\alpha_1 t}\boldsymbol{f}(t)$, $\boldsymbol{w}_{\alpha_1}(t)=\boldsymbol{e}^{\alpha_1 t}\boldsymbol{w}(t)$, $\boldsymbol{y}_{\alpha_1}(t)=\boldsymbol{e}^{\alpha_1(t-\tau(t))}\boldsymbol{y}(t)$, $\boldsymbol{v}_{\alpha_1}(t-\tau(t))=\boldsymbol{e}^{\alpha_1(t-\tau(t))}\boldsymbol{v}(t-\tau(t))$.

$$\bar{\boldsymbol{y}}(t)=\begin{cases}\boldsymbol{y}_{\alpha_1}(t-\tau(t)), & \lambda=0,\\ \boldsymbol{y}_{\alpha_1\mathrm{pre}}(t-\tau(t)), & \lambda=1.\end{cases} \tag{15}$$

By introducing a state transition $\hat{\boldsymbol{x}}(t)=\boldsymbol{e}^{-\alpha_1 t}\hat{\boldsymbol{\zeta}}(t)$, the state and fault estimation observer with α-stability can be designed as

$$\begin{cases}\dot{\hat{\boldsymbol{\zeta}}}(t)=\tilde{\boldsymbol{A}}\hat{\boldsymbol{\zeta}}(t)+\boldsymbol{B}\boldsymbol{u}_{\alpha_1}(t)+\boldsymbol{E}_f\hat{\boldsymbol{f}}_{\alpha_1}(t)-\\ \qquad\boldsymbol{e}^{\alpha_1\tau(t)}\boldsymbol{L}\left[\hat{\boldsymbol{y}}_{\alpha_1}(t)-\bar{\boldsymbol{y}}_{\alpha_1}(t)\right],\\ \hat{\boldsymbol{y}}_{\alpha_1}(t)=\boldsymbol{C}\hat{\boldsymbol{\zeta}}(t-\tau(t)),\\ \dot{\hat{\boldsymbol{f}}}_{\alpha_1}(t)=-\boldsymbol{e}^{\alpha_1\tau(t)}\boldsymbol{F}\left[\hat{\boldsymbol{y}}_{\alpha_1}(t)-\bar{\boldsymbol{y}}_{\alpha_1}(t)\right],\end{cases} \tag{16}$$

where $\hat{\boldsymbol{\zeta}}(t)\in\mathbf{R}^n$ and $\hat{\boldsymbol{y}}_{\alpha_1}(t)\in\mathbf{R}^m$ are system state estimation value and observer output value, respectively; $\hat{\boldsymbol{f}}_{\alpha_1}(t)$ is fault estimation value; $\boldsymbol{L},\boldsymbol{F}$ are observer gain matrix and fault gain matrix, respectively.

Define $\begin{cases}\boldsymbol{e}_{x\alpha_1}(t)=\hat{\boldsymbol{\zeta}}(t)-\boldsymbol{\zeta}(t),\\ \boldsymbol{e}_{y\alpha_1}(t)=\hat{\boldsymbol{y}}_{\alpha_1}(t)-\bar{\boldsymbol{y}}_{\alpha_1}(t),\\ \boldsymbol{e}_{f\alpha_1}(t)=\hat{\boldsymbol{f}}_{\alpha_1}(t)-\boldsymbol{f}_{\alpha_1}(t),\end{cases}$ and the error system can be obtained by

$$\begin{cases}\dot{\boldsymbol{e}}_{x\alpha_1}(t)=\tilde{\boldsymbol{A}}\boldsymbol{e}_{x\alpha_1}(t)+\boldsymbol{E}_f\boldsymbol{e}_{f\alpha_1}(t)-\boldsymbol{B}_w\boldsymbol{w}_{\alpha_1}(t)-\\ \qquad\boldsymbol{L}\boldsymbol{C}\boldsymbol{e}^{\alpha_1\tau(t)}\boldsymbol{e}_{x\alpha_1}(t-\tau(t))+\\ \qquad\boldsymbol{L}\boldsymbol{E}_v\boldsymbol{e}^{\alpha_1\tau(t)}\boldsymbol{v}_{\alpha_1}(t-\tau(t)),\\ \boldsymbol{e}_{y\alpha_1}(t)=\boldsymbol{C}\boldsymbol{e}_{x\alpha_1}(t-\tau(t))-\boldsymbol{E}_v\boldsymbol{v}_{\alpha_1}(t-\tau(t)).\end{cases} \tag{17}$$

The derivative of fault estimation error with respect to time is

$$\begin{aligned}\dot{\boldsymbol{e}}_{f\alpha_1}(t)=&-\boldsymbol{e}^{\alpha_1\tau(t)}\boldsymbol{F}\boldsymbol{C}\boldsymbol{e}_{x\alpha_1}(t-\tau(t))+\\ &\boldsymbol{e}^{\alpha_1\tau(t)}\boldsymbol{F}\boldsymbol{E}_v\boldsymbol{v}_{\alpha_1}(t-\tau(t))-\dot{\boldsymbol{f}}_{\alpha_1}(t).\end{aligned} \tag{18}$$

Combining Eqs. (17) and (18), the augmented error system can be obtained, that is

$$\begin{aligned}\dot{\bar{\boldsymbol{e}}}_{\alpha_1}(t)=&\bar{\boldsymbol{A}}\bar{\boldsymbol{e}}_{\alpha_1}(t)-\bar{\boldsymbol{L}}\bar{\boldsymbol{C}}\boldsymbol{e}^{\alpha_1\tau(t)}\bar{\boldsymbol{e}}_{\alpha_1}(t-\tau(t))-\\ &\bar{\boldsymbol{B}}_w\bar{\boldsymbol{w}}_{\alpha_1}(t)+\bar{\boldsymbol{L}}\boldsymbol{E}_v\boldsymbol{e}^{\alpha_1\tau(t)}\boldsymbol{v}_{\alpha_1}(t-\tau(t)),\end{aligned} \tag{19}$$

where

$$\bar{\boldsymbol{A}}=\begin{bmatrix}\tilde{\boldsymbol{A}} & \boldsymbol{E}_f\\ \boldsymbol{0} & \boldsymbol{0}\end{bmatrix},\ \bar{\boldsymbol{C}}=\begin{bmatrix}\boldsymbol{C} & \boldsymbol{0}\end{bmatrix},\bar{\boldsymbol{L}}=\begin{bmatrix}\boldsymbol{L}\\ \boldsymbol{F}\end{bmatrix},\ \bar{\boldsymbol{B}}_w=\begin{bmatrix}\boldsymbol{B}_w & \boldsymbol{0}\\ \boldsymbol{0} & \boldsymbol{I}\end{bmatrix},$$

$$\bar{\boldsymbol{e}}_{\alpha_1}(t)=\begin{bmatrix}\boldsymbol{e}_{x\alpha_1}(t)\\ \boldsymbol{e}_{f\alpha_1}(t)\end{bmatrix},\ \bar{\boldsymbol{w}}_{\alpha_1}(t)=\begin{bmatrix}\boldsymbol{w}_{\alpha_1}(t)\\ \dot{\boldsymbol{f}}_{\alpha_1}(t)\end{bmatrix}.$$

The Lyapunov-krasovskii functional is constructed by

$$\boldsymbol{V}(t)=\boldsymbol{V}_1(t)+\boldsymbol{V}_2(t)+\boldsymbol{V}_3(t)+\boldsymbol{V}_4(t), \tag{20}$$

where

$$\boldsymbol{V}_1(t)=\bar{\boldsymbol{e}}_{\alpha_1}^T(t)\boldsymbol{P}\bar{\boldsymbol{e}}_{\alpha_1}(t),$$

$$\boldsymbol{V}_2(t)=\int_{t-\bar{h}}^{t}\bar{\boldsymbol{e}}_{\alpha_1}^T(s)\boldsymbol{Q}\bar{\boldsymbol{e}}_{\alpha_1}(s)\mathrm{d}s,$$

$$\boldsymbol{V}_3(t)=\int_{-\bar{h}}^{0}\int_{t+\theta}^{t}\dot{\bar{\boldsymbol{e}}}_{\alpha_1}^T(s)\boldsymbol{Z}\dot{\bar{\boldsymbol{e}}}_{\alpha_1}(s)\mathrm{d}s\,\mathrm{d}\theta,$$

$$\boldsymbol{V}_4(t)=\bar{h}^2\int_{t-\tau(t)}^{t}\dot{\bar{\boldsymbol{e}}}_{\alpha_1}^T(s)\boldsymbol{R}\dot{\bar{\boldsymbol{e}}}_{\alpha_1}(s)\mathrm{d}s-\int_{t-\tau(t)}^{t}\boldsymbol{\varphi}_1^T(s)\boldsymbol{R}\boldsymbol{\varphi}_1(s)\mathrm{d}s,$$

where $\boldsymbol{\varphi}_1(t)=\bar{\boldsymbol{e}}_{\alpha_1}(t)-\bar{\boldsymbol{e}}_{\alpha_1}(t-\tau(t))$ and $\boldsymbol{P},\boldsymbol{Q},\boldsymbol{R},\boldsymbol{Z}$ are positive definite symmetric matrices.

Under zero initial conditions, consider making the error system (19) asymptotically stable, let $\bar{\boldsymbol{w}}(t)=0$, $\boldsymbol{v}(t-\tau(t))=0$, and take the derivative of $\boldsymbol{V}(t)$ along this system to get

$$\dot{\boldsymbol{V}}(t)=\dot{\boldsymbol{V}}_1(t)+\dot{\boldsymbol{V}}_2(t)+\dot{\boldsymbol{V}}_3(t)+\dot{\boldsymbol{V}}_4(t), \tag{21}$$

where

$$\dot{\boldsymbol{V}}_1(t)=2\bar{\boldsymbol{e}}_{\alpha_1}^{\mathrm{T}}(t)\boldsymbol{P}\dot{\bar{\boldsymbol{e}}}_{\alpha_1}(t),$$

$$\dot{\boldsymbol{V}}_2(t)=\bar{\boldsymbol{e}}_{\alpha_1}^{\mathrm{T}}(t)\boldsymbol{Q}\bar{\boldsymbol{e}}_{\alpha_1}(t)-\bar{\boldsymbol{e}}_{\alpha_1}^{\mathrm{T}}(t-\bar{h})\boldsymbol{Q}\bar{\boldsymbol{e}}_{\alpha_1}(t-\bar{h}),$$

$$\dot{\boldsymbol{V}}_3(t)=\bar{h}\dot{\bar{\boldsymbol{e}}}_{\alpha_1}^{\mathrm{T}}(t)\boldsymbol{Z}\dot{\bar{\boldsymbol{e}}}_{\alpha_1}(t)-\int_{t-\bar{h}}^{t}\dot{\bar{\boldsymbol{e}}}_{\alpha_1}^{\mathrm{T}}(s)\boldsymbol{Z}\dot{\bar{\boldsymbol{e}}}_{\alpha_1}(s)\mathrm{d}s,$$

$$\dot{\boldsymbol{V}}_4(t)=\bar{h}^2\dot{\bar{\boldsymbol{e}}}_{\alpha_1}^{\mathrm{T}}(t)\boldsymbol{R}\dot{\bar{\boldsymbol{e}}}_{\alpha_1}(t)+\bar{\boldsymbol{e}}_{\alpha_1}^{\mathrm{T}}(t-\tau(t))\boldsymbol{R}\bar{\boldsymbol{e}}_{\alpha_1}(t-\tau(t))-\bar{\boldsymbol{e}}_{\alpha_1}^{\mathrm{T}}(t)\boldsymbol{R}\bar{\boldsymbol{e}}_{\alpha_1}(t).$$

A new type of B-L inequality is used to deal with the integral term in $\boldsymbol{V}_3(t)$, namely

$$-\int_{t-\bar{h}}^{t}\dot{\bar{\boldsymbol{e}}}_{\alpha_1}^{T}(s)\boldsymbol{Z}\dot{\bar{\boldsymbol{e}}}_{\alpha_1}(s)\mathrm{d}s\leqslant\boldsymbol{\varsigma}_1^{\mathrm{T}}\left[\mathrm{Sym}\left\{\boldsymbol{\Pi}^{\mathrm{T}}\boldsymbol{M}\right\}+\bar{h}\boldsymbol{M}^{\mathrm{T}}\tilde{\boldsymbol{R}}\boldsymbol{M}\right]\boldsymbol{\varsigma}_1, \tag{22}$$

where

$$\boldsymbol{\varsigma}_1=\left[\bar{\boldsymbol{e}}_{\alpha_1}(t)\quad\bar{\boldsymbol{e}}_{\alpha_1}(t-\bar{h})\quad\boldsymbol{\gamma}_1\quad\boldsymbol{\gamma}_2\quad\bar{\boldsymbol{e}}_{\alpha_1}(t-\tau(t))\right]^{\mathrm{T}},$$

$$\boldsymbol{\gamma}_1=\int_{t-\bar{h}}^{t}\frac{\bar{\boldsymbol{e}}_{\alpha_1}(s)}{\bar{h}}\mathrm{d}s,\ \boldsymbol{\gamma}_2=\int_{t-\bar{h}}^{t}\frac{(t-s)\bar{\boldsymbol{e}}_{\alpha_1}(s)}{\bar{h}^2}\mathrm{d}s,$$

$$\boldsymbol{\Pi}=\begin{bmatrix}\boldsymbol{I} & -\boldsymbol{I} & \boldsymbol{0} & \boldsymbol{0} & \boldsymbol{0}\\ \boldsymbol{I} & \boldsymbol{I} & -2\boldsymbol{I} & \boldsymbol{0} & \boldsymbol{0}\\ \boldsymbol{I} & -\boldsymbol{I} & -6\boldsymbol{I} & 12\boldsymbol{I} & \boldsymbol{0}\end{bmatrix},\tilde{\boldsymbol{R}}=\begin{bmatrix}\boldsymbol{Z} & \boldsymbol{0} & \boldsymbol{0}\\ \boldsymbol{0} & 3\boldsymbol{Z} & \boldsymbol{0}\\ \boldsymbol{0} & \boldsymbol{0} & 5\boldsymbol{Z}\end{bmatrix}.$$

Put the Eq. (22) into Eq. (21), and record $\boldsymbol{M}_{11}=\begin{bmatrix}\boldsymbol{I} & \boldsymbol{0} & \boldsymbol{0} & \boldsymbol{0} & \boldsymbol{0}\end{bmatrix}$, $\boldsymbol{M}_{12}=\begin{bmatrix}\bar{\boldsymbol{A}} & \boldsymbol{0} & \boldsymbol{0} & \boldsymbol{0} & -\boldsymbol{e}^{\alpha_1\tau(t)}\bar{\boldsymbol{L}}\bar{\boldsymbol{C}}\end{bmatrix}$, $\boldsymbol{M}_{13}=\begin{bmatrix}\boldsymbol{0} & \boldsymbol{I} & \boldsymbol{0} & \boldsymbol{0} & \boldsymbol{0}\end{bmatrix}$, $\boldsymbol{M}_{14}=\begin{bmatrix}\boldsymbol{0} & \boldsymbol{0} & \boldsymbol{0} & \boldsymbol{0} & \boldsymbol{I}\end{bmatrix}$, then there are $\bar{\boldsymbol{e}}_{\alpha_1}(t)=\boldsymbol{M}_{11}\boldsymbol{\varsigma}_1$, $\dot{\bar{\boldsymbol{e}}}_{\alpha_1}(t)=\boldsymbol{M}_{12}\boldsymbol{\varsigma}_1$, $\bar{\boldsymbol{e}}_{\alpha_1}(t-\bar{h})=\boldsymbol{M}_{13}\boldsymbol{\varsigma}_1$, $\bar{\boldsymbol{e}}_{\alpha_1}(t-\tau(t))=\boldsymbol{M}_{14}\boldsymbol{\varsigma}_1$.

Therefore, it can be obtained that

$$\dot{\boldsymbol{V}}(t)\leqslant\boldsymbol{\varsigma}_1^{\mathrm{T}}\boldsymbol{\Sigma}_1\boldsymbol{\varsigma}_1, \tag{23}$$

where

$$\boldsymbol{\Sigma}_1=\boldsymbol{M}_{11}^{\mathrm{T}}\boldsymbol{P}\boldsymbol{M}_{12}+\boldsymbol{M}_{12}^{\mathrm{T}}\boldsymbol{P}\boldsymbol{M}_{11}+\boldsymbol{M}_{11}^{\mathrm{T}}\boldsymbol{Q}\boldsymbol{M}_{11}-\boldsymbol{M}_{13}^{\mathrm{T}}\boldsymbol{Q}\boldsymbol{M}_{13}+h\boldsymbol{M}_{12}^{\mathrm{T}}\boldsymbol{Z}\boldsymbol{M}_{12}+\boldsymbol{\Pi}^{\mathrm{T}}\boldsymbol{M}+\boldsymbol{M}^{\mathrm{T}}\boldsymbol{\Pi}+h\boldsymbol{M}\tilde{\boldsymbol{R}}\boldsymbol{M}^{\mathrm{T}}+\boldsymbol{M}_{14}^{\mathrm{T}}\boldsymbol{R}\boldsymbol{M}_{14}-\boldsymbol{M}_{11}^{\mathrm{T}}\boldsymbol{R}\boldsymbol{M}_{11}+h^2\boldsymbol{M}_{12}^{\mathrm{T}}\boldsymbol{R}\boldsymbol{M}_{12}.$$

If $\boldsymbol{\Sigma}_1<0$ holds, then $\dot{\boldsymbol{V}}(t)<0$, according to the Lyapunov stability theory, we know that the error system (19) is asymptotically stable, that is, it has α-stability.

Under zero initial conditions, when $\boldsymbol{v}(t-\tau(t))\neq0$, $\bar{\boldsymbol{w}}(t)\neq0$, consider the H_∞ performance indicators

$$J_1=\dot{V}(t)+\bar{\boldsymbol{e}}_{a_1}^{\mathrm{T}}(t)\bar{\boldsymbol{e}}_{a_1}(t)-\gamma_1^2\bar{\boldsymbol{w}}_{a_1}^{\mathrm{T}}(t)\bar{\boldsymbol{w}}_{a_1}(t)-\gamma_1^2\boldsymbol{v}_{a_1}^{\mathrm{T}}(t-\tau(t))\boldsymbol{v}_{a_1}(t-\tau(t))<0, \tag{24}$$

denoted by

$$\boldsymbol{\varsigma}_2=\left[\bar{\boldsymbol{e}}_{a_1}(t)\ \ \bar{\boldsymbol{e}}_{a_1}(t-\bar{h})\ \ \boldsymbol{\gamma}_1\ \ \boldsymbol{\gamma}_2\ \ \bar{\boldsymbol{e}}_{a_1}(t-\tau(t))\ \ \boldsymbol{v}_{a_1}(t-\tau(t))\ \ \bar{\boldsymbol{w}}_{a_1}(t)\right]^{\mathrm{T}},$$

$$\boldsymbol{M}_{21}=\left[\boldsymbol{I}\ \ 0\ \ 0\ \ 0\ \ 0\ \ 0\ \ 0\right],$$

$$\boldsymbol{M}_{22}=\left[\bar{\boldsymbol{A}}\ \ 0\ \ 0\ \ 0\ \ -\boldsymbol{e}^{\alpha_1\tau(t)}\bar{\boldsymbol{L}}\bar{\boldsymbol{C}}\ \ \boldsymbol{e}^{\alpha_1\tau(t)}\bar{\boldsymbol{L}}\boldsymbol{E}_v\ \ -\bar{\boldsymbol{B}}_w\right],$$

$$\boldsymbol{M}_{23}=\left[0\ \ \boldsymbol{I}\ \ 0\ \ 0\ \ 0\ \ 0\ \ 0\right],$$

$$\boldsymbol{M}_{24}=\left[0\ \ 0\ \ 0\ \ 0\ \ \boldsymbol{I}\ \ 0\ \ 0\right],$$

$$\boldsymbol{M}_{25}=\begin{bmatrix}\boldsymbol{I}&0&0&0&0&0&0\\0&\boldsymbol{I}&0&0&0&0&0\\0&0&\boldsymbol{I}&0&0&0&0\\0&0&0&\boldsymbol{I}&0&0&0\\0&0&0&0&\boldsymbol{I}&0&0\end{bmatrix},$$

$$\boldsymbol{M}_{26}=\begin{bmatrix}0&0&0&0&0&\boldsymbol{I}&0\\0&0&0&0&0&0&\boldsymbol{I}\end{bmatrix}.$$

Then there is $\bar{\boldsymbol{e}}_{a_1}(t)=\boldsymbol{M}_{21}\boldsymbol{\varsigma}_2$, $\dot{\bar{\boldsymbol{e}}}_{a_1}(t)=\boldsymbol{M}_{22}\boldsymbol{\varsigma}_2$, $\bar{\boldsymbol{e}}_{a_1}(t-\bar{h})=\boldsymbol{M}_{23}\boldsymbol{\varsigma}_2$, $\bar{\boldsymbol{e}}_{a_1}(t-\tau(t))=\boldsymbol{M}_{24}\boldsymbol{\varsigma}_2$, $\boldsymbol{\varsigma}_1=\boldsymbol{M}_{25}\boldsymbol{\varsigma}_2$, $\left[\boldsymbol{v}_{a_1}(t-\tau(t))\ \ \bar{\boldsymbol{w}}_{a_1}(t)\right]^{\mathrm{T}}=\boldsymbol{M}_{26}\boldsymbol{\varsigma}_2$.

Therefore, it can be obtained that

$$J_1\leqslant\boldsymbol{\varsigma}_2^{\mathrm{T}}\boldsymbol{\Sigma}_2\boldsymbol{\varsigma}_2<0, \tag{25}$$

where

$$\boldsymbol{\Sigma}_2=\boldsymbol{M}_{21}^{\mathrm{T}}\boldsymbol{P}\boldsymbol{M}_{22}+\boldsymbol{M}_{22}^{\mathrm{T}}\boldsymbol{P}\boldsymbol{M}_{21}+\boldsymbol{M}_{21}^{\mathrm{T}}\boldsymbol{Q}\boldsymbol{M}_{21}-\boldsymbol{M}_{23}^{\mathrm{T}}\boldsymbol{Q}\boldsymbol{M}_{23}+h\boldsymbol{M}_{22}^{\mathrm{T}}\boldsymbol{Z}\boldsymbol{M}_{22}+\boldsymbol{M}_{25}^{\mathrm{T}}(\boldsymbol{\Pi}^{\mathrm{T}}\boldsymbol{M}+\boldsymbol{M}^{\mathrm{T}}\boldsymbol{\Pi}+h\boldsymbol{M}\tilde{\boldsymbol{R}}\boldsymbol{M}^{\mathrm{T}})\boldsymbol{M}_{25}+\boldsymbol{M}_{24}^{\mathrm{T}}\boldsymbol{R}\boldsymbol{M}_{24}-\boldsymbol{M}_{21}^{\mathrm{T}}\boldsymbol{R}\boldsymbol{M}_{21}+h^2\boldsymbol{M}_{22}^{\mathrm{T}}\boldsymbol{R}\boldsymbol{M}_{22}+\boldsymbol{M}_{21}^{\mathrm{T}}\boldsymbol{M}_{21}-\gamma_1^2\boldsymbol{M}_{26}^{\mathrm{T}}\boldsymbol{M}_{26}.$$

According to the Lyapunov stability theory, if $\boldsymbol{\Sigma}_2<0$ holds true, then Eq. (25) holds true, that is, the dynamic error system (19) satisfies the performance index (24).

Based on the above deduction, the dynamic error system (19) has α-stability and H_∞ performance indicators, if and only if the following matrix inequalities are established.

$$\begin{cases}\boldsymbol{\Sigma}_1<0,\\ \boldsymbol{\Sigma}_2<0.\end{cases} \tag{26}$$

Expand Eq. (26) and set $\boldsymbol{Y}=\boldsymbol{P}\bar{\boldsymbol{L}}$, and apply Schur's lemma to get Eqs. (12) and (13), respectively.

Integrating Eq. (24) from 0 to $+\infty$, it can be obtained that

$$V(+\infty)-V(0)\leqslant-\int_0^{+\infty}\bar{\boldsymbol{e}}_{a_1}^{\mathrm{T}}(t)\bar{\boldsymbol{e}}_{a_1}(t)\mathrm{d}t+\gamma_1^2\int_0^{+\infty}\bar{\boldsymbol{w}}_{a_1}^{\mathrm{T}}(t)\bar{\boldsymbol{w}}_{a_1}(t)\mathrm{d}t+\gamma_1^2\sum_{k=0}^{+\infty}(j_{k+1}-j_k)\boldsymbol{v}_{a_1}^{\mathrm{T}}(j_k)\boldsymbol{v}_{a_1}(j_k),$$

where $V(0)=0$, $V(+\infty)\geqslant0$, $\bar{\boldsymbol{w}}_{a_1}(t)\in L_2[0,\infty)$, $\boldsymbol{v}_{a_1}(j_k)\in L_2[0,\infty)$, then there is

$$\int_0^{+\infty}\bar{\boldsymbol{e}}_{a_1}^{\mathrm{T}}(t)\bar{\boldsymbol{e}}_{a_1}(t)\mathrm{d}t\leqslant\gamma_1^2\int_0^{+\infty}\bar{\boldsymbol{w}}_{a_1}^{\mathrm{T}}(t)\bar{\boldsymbol{w}}_{a_1}(t)\mathrm{d}t+\gamma_1^2\sum_{k=0}^{+\infty}(j_{k+1}-j_k)\boldsymbol{v}_{a_1}^{\mathrm{T}}(j_k)\boldsymbol{v}_{a_1}(j_k).$$

Namely,

$$\left\|\bar{\boldsymbol{e}}_{a_1}(t)\right\|_2^2\leqslant\gamma_1^2\left[\left\|\bar{\boldsymbol{w}}_{a_1}(t)\right\|_2^2+\sum_{k=0}^{+\infty}(j_{k+1}-j_k)\left\|\boldsymbol{v}_{a_1}(j_k)\right\|_2^2\right].$$

In summary, **Theorem 1** has been proved.

In addition, there are nonlinear terms in the inequalities (12) and (13) in **Theorem 1**, which cannot be directly solved by the LMI toolbox in MATLAB. Here, the cone complement linearization algorithm will be introduced to obtain the observer parameters. Select the appropriate dimension matrix $\boldsymbol{G},\boldsymbol{T}$, so that $\boldsymbol{P}\boldsymbol{R}^{-1}\boldsymbol{P}\geqslant\boldsymbol{G},\boldsymbol{P}\boldsymbol{Z}^{-1}\boldsymbol{P}\geqslant\boldsymbol{T}$ holds true, then the matrix inequalities (12) and (13) can be transformed into

$$\begin{bmatrix}\boldsymbol{U}_{11}&\boldsymbol{U}_{12}&\boldsymbol{U}_{13}&\boldsymbol{U}_{14}&\boldsymbol{U}_{15}&\boldsymbol{M}^{\mathrm{T}}&\boldsymbol{U}_{17}&\boldsymbol{U}_{18}\\*&\boldsymbol{U}_{22}&\boldsymbol{U}_{23}&\boldsymbol{U}_{24}&\boldsymbol{U}_{25}&\boldsymbol{M}^{\mathrm{T}}&0&0\\*&*&\boldsymbol{U}_{33}&\boldsymbol{U}_{34}&\boldsymbol{U}_{35}&\boldsymbol{M}^{\mathrm{T}}&0&0\\*&*&*&\boldsymbol{U}_{44}&\boldsymbol{U}_{45}&\boldsymbol{M}^{\mathrm{T}}&0&0\\*&*&*&*&\boldsymbol{U}_{55}&\boldsymbol{M}^{\mathrm{T}}&\boldsymbol{U}_{57}&\boldsymbol{U}_{58}\\*&*&*&*&*&\boldsymbol{U}_{66}&0&0\\*&*&*&*&*&*&-\boldsymbol{G}&0\\*&*&*&*&*&*&*&-\boldsymbol{T}\end{bmatrix}<0, \tag{27}$$

$$\begin{bmatrix}\boldsymbol{V}_{11}&\boldsymbol{V}_{12}&\boldsymbol{V}_{13}&\boldsymbol{V}_{14}&\boldsymbol{V}_{15}&\boldsymbol{V}_{16}&\boldsymbol{V}_{17}&\boldsymbol{M}^{\mathrm{T}}&\boldsymbol{V}_{19}&\boldsymbol{V}_{110}\\*&\boldsymbol{V}_{22}&\boldsymbol{V}_{23}&\boldsymbol{V}_{24}&\boldsymbol{V}_{25}&0&0&\boldsymbol{M}^{\mathrm{T}}&0&0\\*&*&\boldsymbol{V}_{33}&\boldsymbol{V}_{34}&\boldsymbol{V}_{35}&0&0&\boldsymbol{M}^{\mathrm{T}}&0&0\\*&*&*&\boldsymbol{V}_{44}&\boldsymbol{V}_{45}&0&0&\boldsymbol{M}^{\mathrm{T}}&0&0\\*&*&*&*&\boldsymbol{V}_{55}&0&0&\boldsymbol{M}^{\mathrm{T}}&\boldsymbol{V}_{59}&\boldsymbol{V}_{510}\\*&*&*&*&*&\boldsymbol{V}_{66}&0&0&\boldsymbol{V}_{69}&\boldsymbol{V}_{610}\\*&*&*&*&*&*&\boldsymbol{V}_{77}&0&\boldsymbol{V}_{79}&\boldsymbol{V}_{710}\\*&*&*&*&*&*&*&\boldsymbol{V}_{88}&0&0\\*&*&*&*&*&*&*&*&-\boldsymbol{G}&0\\*&*&*&*&*&*&*&*&*&-\boldsymbol{T}\end{bmatrix}<0. \tag{28}$$

Transform the formula $\boldsymbol{P}\boldsymbol{R}^{-1}\boldsymbol{P}\geqslant\boldsymbol{G},\boldsymbol{P}\boldsymbol{Z}^{-1}\boldsymbol{P}\geqslant\boldsymbol{T}$ into $\begin{cases}\boldsymbol{G}^{-1}\geqslant\boldsymbol{P}^{-1}\boldsymbol{R}\boldsymbol{P}^{-1}\\ \boldsymbol{T}^{-1}\geqslant\boldsymbol{P}^{-1}\boldsymbol{Z}\boldsymbol{P}^{-1}\end{cases}$, apply Schur's complement lemma to it and set $\boldsymbol{G}^{-1}=\bar{\boldsymbol{G}},\boldsymbol{P}^{-1}=\bar{\boldsymbol{P}},\boldsymbol{R}^{-1}=\bar{\boldsymbol{R}},\boldsymbol{T}^{-1}=\bar{\boldsymbol{T}},\boldsymbol{Z}^{-1}=\bar{\boldsymbol{Z}}$. The inequality constraint group can be obtained by

$$\begin{cases}\begin{bmatrix}\bar{\boldsymbol{G}}&\bar{\boldsymbol{P}}\\\bar{\boldsymbol{P}}&\bar{\boldsymbol{R}}\end{bmatrix}\geqslant0,\begin{bmatrix}\boldsymbol{G}&\boldsymbol{I}\\\boldsymbol{I}&\bar{\boldsymbol{G}}\end{bmatrix}\geqslant0,\begin{bmatrix}\boldsymbol{P}&\boldsymbol{I}\\\boldsymbol{I}&\bar{\boldsymbol{P}}\end{bmatrix}\geqslant0,\\ \begin{bmatrix}\boldsymbol{R}&\boldsymbol{I}\\\boldsymbol{I}&\bar{\boldsymbol{R}}\end{bmatrix}\geqslant0,\begin{bmatrix}\bar{\boldsymbol{T}}&\bar{\boldsymbol{P}}\\\bar{\boldsymbol{P}}&\bar{\boldsymbol{Z}}\end{bmatrix}\geqslant0,\begin{bmatrix}\boldsymbol{T}&\boldsymbol{I}\\\boldsymbol{I}&\bar{\boldsymbol{T}}\end{bmatrix}\geqslant0,\\ \begin{bmatrix}\boldsymbol{Z}&\boldsymbol{I}\\\boldsymbol{I}&\bar{\boldsymbol{Z}}\end{bmatrix}\geqslant0.\end{cases} \tag{29}$$

Using the cone complement linearization algorithm, the problem of solving the observer can be transformed into the minimization problem with the constraints of the LMI

group.

$$\min Tr(\boldsymbol{G}\bar{\boldsymbol{G}}+\boldsymbol{T}\bar{\boldsymbol{T}}+\boldsymbol{P}\bar{\boldsymbol{P}}+\boldsymbol{R}\bar{\boldsymbol{R}}+\boldsymbol{Z}\bar{\boldsymbol{Z}}). \tag{30}$$

The steps to solve the minimization problem are given below.

1) Obtain a set of feasible solutions satisfying inequalities (27), (28), and (29), and denote as $(\boldsymbol{P}_0,\boldsymbol{Q}_0,\boldsymbol{R}_0,\boldsymbol{Z}_0,\boldsymbol{S}_0,\boldsymbol{G}_0,\bar{\boldsymbol{G}}_0,\bar{\boldsymbol{R}}_0,\bar{\boldsymbol{P}}_0,\boldsymbol{T}_0,\bar{\boldsymbol{T}}_0,\bar{\boldsymbol{Z}}_0,\boldsymbol{Y}_0)$. Verify whether the obtained optimal solution satisfies the inequalities (12) and (13), if so, the solution is obtained; if not, set $k=0$ and execute step 2.

2) Solve the minimization problem with LMI group constraints.

$$\min Tr(\boldsymbol{G}_k\bar{\boldsymbol{G}}+\bar{\boldsymbol{G}}_k\boldsymbol{G}+\boldsymbol{P}_k\bar{\boldsymbol{P}}+\bar{\boldsymbol{P}}_k\boldsymbol{P}+\boldsymbol{R}_k\bar{\boldsymbol{R}}+\bar{\boldsymbol{R}}_k\boldsymbol{R}+\boldsymbol{T}_k\bar{\boldsymbol{T}}+\bar{\boldsymbol{T}}_k\boldsymbol{T}+\boldsymbol{Z}_k\bar{\boldsymbol{Z}}+\bar{\boldsymbol{Z}}_k\boldsymbol{Z}).$$

Let Eqs. (27), (28), and (29) remain unchanged. Let the optimal solution obtained be $(\boldsymbol{G}_{k+1},\bar{\boldsymbol{G}}_{k+1},\boldsymbol{P}_{k+1},\bar{\boldsymbol{P}}_{k+1},\boldsymbol{R}_{k+1},\bar{\boldsymbol{R}}_{k+1},\boldsymbol{T}_{k+1},\bar{\boldsymbol{T}}_{k+1},\boldsymbol{Z}_{k+1},\bar{\boldsymbol{Z}}_{k+1})$.

3) Verify whether the obtained optimal solution satisfies the inequalities (14) and (15), and if so, the solution is obtained. If not, check whether k has reached the specified number of iterations, if so, there is no solution; otherwise, set $k=k+1$, go back to step 2.

4 Design of integrated safety controller with multi-objective constraints

Under the limited energy DoS attacks, according to the state and fault values estimated in the previous section, the integrated security controller with active and passive tolerance of DoS attacks and active fault tolerance is designed as

$$\boldsymbol{u}(t)=\boldsymbol{K}\hat{\boldsymbol{x}}(t-\tau(t))-\boldsymbol{B}^{+}\boldsymbol{E}_f\hat{\boldsymbol{f}}(t-\tau(t)), \tag{31}$$

where $t\in[j_k,j_{k+1})$; $\boldsymbol{K}\in\mathbf{R}^{n_u\times n}$ is the controller gain matrix; $\boldsymbol{B}^{+}\in\mathbf{R}^{n_u\times n}$ is the fault adjustment matrix, which satisfies $(\boldsymbol{I}-\boldsymbol{B}\boldsymbol{B}^{+})\boldsymbol{E}_f=0$.

Putting Eq. (31) into the state equation of Eq. (3), the closed-loop CPS model can be obtained by

$$\dot{\boldsymbol{x}}(t)=\boldsymbol{A}\boldsymbol{x}(t)+\boldsymbol{B}\boldsymbol{K}\boldsymbol{x}(t-\tau(t))+\boldsymbol{B}\boldsymbol{K}\boldsymbol{e}_x(t-\tau(t))-\boldsymbol{E}_f\boldsymbol{e}_f(t-\tau(t))+\boldsymbol{B}_w\boldsymbol{w}(t)+\tau(t)\boldsymbol{E}_f\dot{\boldsymbol{f}}(t). \tag{32}$$

Theorem 2 Given positive numbers $\bar{h},\gamma_2,\sigma,\alpha_2$, if there are positive definite symmetric matrixes $\bar{\boldsymbol{P}},\bar{\boldsymbol{Q}},\bar{\boldsymbol{R}},\bar{\boldsymbol{Z}}$ and matrices $\tilde{\boldsymbol{M}},\bar{\boldsymbol{K}},\boldsymbol{Q}_1,\boldsymbol{Q}_3,\boldsymbol{Q}_5$ of appropriate dimension, satisfying Eqs. (33) — (35), then there is a controller gain $\boldsymbol{K}$ and an event trigger weight matrix $\boldsymbol{\Phi}$, which can make the closed-loop system α_2-asymptotically stable for DoS attacks at different energy levels and meet the performance indicators

$$\|\boldsymbol{\xi}(t)\|_2^2\leqslant\gamma_2^2\left[\|\bar{\boldsymbol{w}}_{\alpha_2}(t)\|_2^2+\sum_{k=0}^{+\infty}(j_{k+1}-j_k)(\|\boldsymbol{e}_{x_{\alpha_2}}(j_k)\|_2^2+\|\boldsymbol{e}_{f_{\alpha_2}}(j_k)\|_2^2)\right].$$

The controller gain $\boldsymbol{K}=(\bar{\boldsymbol{P}}\boldsymbol{B})^{-1}\bar{\boldsymbol{K}}$ and the event trigger weight matrix $\boldsymbol{\Phi}$ can be jointly obtained by

$$\begin{bmatrix}
\boldsymbol{\Gamma}_{11} & \boldsymbol{\Gamma}_{12} & \boldsymbol{\Gamma}_{13} & \boldsymbol{\Gamma}_{14} & \boldsymbol{\Gamma}_{15} & \boldsymbol{M}^{\mathrm{T}} & \boldsymbol{\Gamma}_{17} & \boldsymbol{\Gamma}_{18} & \boldsymbol{\Gamma}_{19} & \boldsymbol{\Gamma}_{110}\\
* & \boldsymbol{\Gamma}_{22} & \boldsymbol{\Gamma}_{23} & \boldsymbol{\Gamma}_{24} & \boldsymbol{\Gamma}_{25} & \boldsymbol{M}^{\mathrm{T}} & 0 & 0 & 0 & 0\\
* & * & \boldsymbol{\Gamma}_{33} & \boldsymbol{\Gamma}_{34} & \boldsymbol{\Gamma}_{35} & \boldsymbol{M}^{\mathrm{T}} & 0 & 0 & 0 & 0\\
* & * & * & \boldsymbol{\Gamma}_{44} & \boldsymbol{\Gamma}_{45} & \boldsymbol{M}^{\mathrm{T}} & 0 & 0 & 0 & 0\\
* & * & * & * & \boldsymbol{\Gamma}_{55} & \boldsymbol{M}^{\mathrm{T}} & \boldsymbol{\Gamma}_{57} & \boldsymbol{\Gamma}_{58} & \boldsymbol{\Gamma}_{59} & \boldsymbol{\Gamma}_{510}\\
* & * & * & * & * & \boldsymbol{\Gamma}_{66} & 0 & 0 & 0 & 0\\
* & * & * & * & * & * & \boldsymbol{\Gamma}_{77} & 0 & 0 & 0\\
* & * & * & * & * & * & * & \boldsymbol{\Gamma}_{88} & 0 & 0\\
* & * & * & * & * & * & * & * & \boldsymbol{\Gamma}_{99} & 0\\
* & * & * & * & * & * & * & * & * & \boldsymbol{\Gamma}_{1010}
\end{bmatrix}<0, \tag{33}$$

$$\begin{bmatrix}
\boldsymbol{\Xi}_{11} & \boldsymbol{\Xi}_{12} & \boldsymbol{\Xi}_{13} & \boldsymbol{\Xi}_{14} & \boldsymbol{\Xi}_{15} & \boldsymbol{\Xi}_{16} & \boldsymbol{\Xi}_{17} & \boldsymbol{\Xi}_{18} & 0 & 0 & \boldsymbol{M}^{\mathrm{T}} & \boldsymbol{\Xi}_{112} & \boldsymbol{\Xi}_{113} & \boldsymbol{\Xi}_{114} & \boldsymbol{\Xi}_{115}\\
* & \boldsymbol{\Xi}_{22} & \boldsymbol{\Xi}_{23} & \boldsymbol{\Xi}_{24} & \boldsymbol{\Xi}_{25} & 0 & 0 & 0 & 0 & 0 & \boldsymbol{M}^{\mathrm{T}} & 0 & 0 & 0 & 0\\
* & * & \boldsymbol{\Xi}_{33} & \boldsymbol{\Xi}_{34} & \boldsymbol{\Xi}_{35} & 0 & 0 & 0 & 0 & 0 & \boldsymbol{M}^{\mathrm{T}} & 0 & 0 & 0 & 0\\
* & * & * & \boldsymbol{\Xi}_{44} & \boldsymbol{\Xi}_{45} & 0 & 0 & 0 & 0 & 0 & \boldsymbol{M}^{\mathrm{T}} & 0 & 0 & 0 & 0\\
* & * & * & * & \boldsymbol{\Xi}_{55} & 0 & 0 & 0 & 0 & 0 & \boldsymbol{M}^{\mathrm{T}} & \boldsymbol{\Xi}_{512} & \boldsymbol{\Xi}_{513} & \boldsymbol{\Xi}_{514} & \boldsymbol{\Xi}_{515}\\
* & * & * & * & * & \boldsymbol{\Xi}_{66} & 0 & 0 & 0 & 0 & 0 & \boldsymbol{\Xi}_{612} & \boldsymbol{\Xi}_{613} & \boldsymbol{\Xi}_{614} & \boldsymbol{\Xi}_{615}\\
* & * & * & * & * & * & \boldsymbol{\Xi}_{77} & 0 & 0 & 0 & 0 & \boldsymbol{\Xi}_{712} & \boldsymbol{\Xi}_{713} & \boldsymbol{\Xi}_{714} & \boldsymbol{\Xi}_{715}\\
* & * & * & * & * & * & * & \boldsymbol{\Xi}_{88} & 0 & 0 & 0 & \boldsymbol{\Xi}_{812} & \boldsymbol{\Xi}_{813} & \boldsymbol{\Xi}_{814} & \boldsymbol{\Xi}_{815}\\
* & * & * & * & * & * & * & * & \boldsymbol{\Xi}_{99} & 0 & 0 & 0 & 0 & 0 & 0\\
* & * & * & * & * & * & * & * & * & \boldsymbol{\Xi}_{1010} & 0 & 0 & 0 & 0 & 0\\
* & * & * & * & * & * & * & * & * & * & \boldsymbol{\Xi}_{1111} & 0 & 0 & 0 & 0\\
* & * & * & * & * & * & * & * & * & * & * & \boldsymbol{\Xi}_{1212} & 0 & 0 & 0\\
* & * & * & * & * & * & * & * & * & * & * & * & \boldsymbol{\Xi}_{1313} & 0 & 0\\
* & * & * & * & * & * & * & * & * & * & * & * & * & \boldsymbol{\Xi}_{1414} & 0\\
* & * & * & * & * & * & * & * & * & * & * & * & * & * & \boldsymbol{\Xi}_{1515}
\end{bmatrix}<0, \tag{34}$$

$$\begin{bmatrix} \boldsymbol{Q}_2 & \boldsymbol{E}_f^{\mathrm{T}}\bar{\boldsymbol{P}} \\ * & \boldsymbol{Q}_1 \end{bmatrix} > 0, \begin{bmatrix} \boldsymbol{Q}_4 & \boldsymbol{E}_f^{\mathrm{T}}\bar{\boldsymbol{R}} \\ * & \boldsymbol{Q}_3 \end{bmatrix} > 0, \begin{bmatrix} \boldsymbol{Q}_6 & \boldsymbol{E}_f^{\mathrm{T}}\bar{\boldsymbol{Z}} \\ * & \boldsymbol{Q}_5 \end{bmatrix} > 0. \tag{35}$$

where

$\boldsymbol{\Gamma}_{11} = \bar{\boldsymbol{P}}\hat{\boldsymbol{A}} + \hat{\boldsymbol{A}}^{\mathrm{T}}\bar{\boldsymbol{P}} + \bar{\boldsymbol{Q}} - \bar{\boldsymbol{R}} + \bar{h}\boldsymbol{Q}_1 + 3\boldsymbol{M} + 3\boldsymbol{M}^{\mathrm{T}}$,
$\boldsymbol{\Gamma}_{12} = 3\boldsymbol{M} - \boldsymbol{M}^{\mathrm{T}}$, $\boldsymbol{\Gamma}_{13} = 3\boldsymbol{M} - 8\boldsymbol{M}^{\mathrm{T}}$,
$\boldsymbol{\Gamma}_{14} = 3\boldsymbol{M} + 12\boldsymbol{M}^{\mathrm{T}}$, $\boldsymbol{\Gamma}_{15} = -\boldsymbol{e}^{\alpha_2\tau(t)}\bar{\boldsymbol{K}} + 3\boldsymbol{M}$,
$\boldsymbol{\Gamma}_{17} = \bar{h}\hat{\boldsymbol{A}}^{\mathrm{T}}\bar{\boldsymbol{P}}$, $\boldsymbol{\Gamma}_{18} = \sqrt{\bar{h}}\,\hat{\boldsymbol{A}}^{\mathrm{T}}\bar{\boldsymbol{P}}$, $\boldsymbol{\Gamma}_{19} = \bar{h}^{\frac{3}{2}}\hat{\boldsymbol{A}}^{\mathrm{T}}\bar{\boldsymbol{P}}$,
$\boldsymbol{\Gamma}_{110} = \bar{h}\hat{\boldsymbol{A}}^{\mathrm{T}}\bar{\boldsymbol{P}}$, $\boldsymbol{\Gamma}_{22} = -\bar{\boldsymbol{Q}} - \boldsymbol{M} - \boldsymbol{M}^{\mathrm{T}}$,
$\boldsymbol{\Gamma}_{23} = -\boldsymbol{M} - 8\boldsymbol{M}^{\mathrm{T}}$, $\boldsymbol{\Gamma}_{24} = -\boldsymbol{M} + 12\boldsymbol{M}^{\mathrm{T}}$,
$\boldsymbol{\Gamma}_{25} = -\boldsymbol{M}$, $\boldsymbol{\Gamma}_{33} = -8\boldsymbol{M} - 8\boldsymbol{M}^{\mathrm{T}}$,
$\boldsymbol{\Gamma}_{34} = -8\boldsymbol{M} + 12\boldsymbol{M}^{\mathrm{T}}$, $\boldsymbol{\Gamma}_{35} = -8\boldsymbol{M}$,
$\boldsymbol{\Gamma}_{44} = 12\boldsymbol{M} + 12\boldsymbol{M}^{\mathrm{T}}$, $\boldsymbol{\Gamma}_{45} = 12\boldsymbol{M}$,
$\boldsymbol{\Gamma}_{55} = \bar{\boldsymbol{R}}$, $\boldsymbol{\Gamma}_{57} = -\bar{h}\boldsymbol{e}^{\alpha_2\tau(t)}\bar{\boldsymbol{K}}^{\mathrm{T}}$,
$\boldsymbol{\Gamma}_{58} = -\sqrt{\bar{h}}\,\boldsymbol{e}^{\alpha_2\tau(t)}\bar{\boldsymbol{K}}^{\mathrm{T}}$, $\boldsymbol{\Gamma}_{59} = -\bar{h}^{\frac{3}{2}}\boldsymbol{e}^{\alpha_2\tau(t)}\bar{\boldsymbol{K}}^{\mathrm{T}}$,
$\boldsymbol{\Gamma}_{510} = -\bar{h}\boldsymbol{e}^{\alpha_2\tau(t)}\bar{\boldsymbol{K}}^{\mathrm{T}}$,
$\boldsymbol{\Gamma}_{66} = \dfrac{1}{-9h}\bar{\boldsymbol{Z}}^{-1}$, $\boldsymbol{\Gamma}_{77} = -\bar{\boldsymbol{P}}\bar{\boldsymbol{R}}^{-1}\bar{\boldsymbol{P}}$, $\boldsymbol{\Gamma}_{88} = -\bar{\boldsymbol{P}}\bar{\boldsymbol{Z}}^{-1}\bar{\boldsymbol{P}}$,
$\boldsymbol{\Gamma}_{99} = -\bar{\boldsymbol{P}}\boldsymbol{Q}_3^{-1}\bar{\boldsymbol{P}}$, $\boldsymbol{\Gamma}_{1010} = -\bar{\boldsymbol{P}}\boldsymbol{Q}_5^{-1}\bar{\boldsymbol{P}}$,
$\boldsymbol{\Xi}_{11} = \bar{\boldsymbol{P}}\hat{\boldsymbol{A}} + \hat{\boldsymbol{A}}^{\mathrm{T}}\bar{\boldsymbol{P}} + \bar{\boldsymbol{Q}} - \bar{\boldsymbol{R}} + \bar{h}\boldsymbol{Q}_1 + \boldsymbol{I} + 3\boldsymbol{M} + 3\boldsymbol{M}^{\mathrm{T}}$,
$\boldsymbol{\Xi}_{12} = 3\boldsymbol{M} - \boldsymbol{M}^{\mathrm{T}}$, $\boldsymbol{\Xi}_{13} = 3\boldsymbol{M} - 8\boldsymbol{M}^{\mathrm{T}}$,
$\boldsymbol{\Xi}_{14} = 3\boldsymbol{M} + 12\boldsymbol{M}^{\mathrm{T}}$, $\boldsymbol{\Xi}_{15} = -\boldsymbol{e}^{\alpha_2\tau(t)}\bar{\boldsymbol{K}} + 3\boldsymbol{M}$,
$\boldsymbol{\Xi}_{16} = -\boldsymbol{e}^{\alpha_2\tau(t)}\bar{\boldsymbol{K}}$, $\boldsymbol{\Xi}_{17} = -\boldsymbol{e}^{\alpha_2\tau(t)}\bar{\boldsymbol{P}}\boldsymbol{E}_f$, $\boldsymbol{\Xi}_{18} = \bar{\boldsymbol{P}}\boldsymbol{E}_w$,
$\boldsymbol{\Xi}_{112} = \bar{h}\hat{\boldsymbol{A}}^{\mathrm{T}}\bar{\boldsymbol{P}}$, $\boldsymbol{\Xi}_{113} = \sqrt{\bar{h}}\,\hat{\boldsymbol{A}}^{\mathrm{T}}\bar{\boldsymbol{P}}$, $\boldsymbol{\Xi}_{114} = \bar{h}^{\frac{3}{2}}\hat{\boldsymbol{A}}^{\mathrm{T}}\bar{\boldsymbol{P}}$,
$\boldsymbol{\Xi}_{115} = \bar{h}\hat{\boldsymbol{A}}^{\mathrm{T}}\bar{\boldsymbol{P}}$, $\boldsymbol{\Xi}_{22} = -\bar{\boldsymbol{Q}} - \boldsymbol{M} - \boldsymbol{M}^{\mathrm{T}}$,
$\boldsymbol{\Xi}_{23} = -\boldsymbol{M} - 8\boldsymbol{M}^{\mathrm{T}}$, $\boldsymbol{\Xi}_{24} = -\boldsymbol{M} + 12\boldsymbol{M}^{\mathrm{T}}$, $\boldsymbol{\Xi}_{25} = -\boldsymbol{M}$,
$\boldsymbol{\Xi}_{33} = -8\boldsymbol{M} - 8\boldsymbol{M}^{\mathrm{T}}$, $\boldsymbol{\Xi}_{34} = -8\boldsymbol{M} + 12\boldsymbol{M}^{\mathrm{T}}$,
$\boldsymbol{\Xi}_{35} = -8\boldsymbol{M}$, $\boldsymbol{\Xi}_{44} = 12\boldsymbol{M} + 12\boldsymbol{M}^{\mathrm{T}}$, $\boldsymbol{\Xi}_{45} = 12\boldsymbol{M}$,
$\boldsymbol{\Xi}_{55} = \bar{\boldsymbol{R}}$, $\boldsymbol{\Xi}_{512} = -\bar{h}\boldsymbol{e}^{\alpha_2\tau(t)}\bar{\boldsymbol{K}}^{\mathrm{T}}$, $\boldsymbol{\Xi}_{513} = -\sqrt{\bar{h}}\,\boldsymbol{e}^{\alpha_2\tau(t)}\bar{\boldsymbol{K}}^{\mathrm{T}}$,
$\boldsymbol{\Xi}_{514} = -\bar{h}^{\frac{3}{2}}\boldsymbol{e}^{\alpha_2\tau(t)}\bar{\boldsymbol{K}}^{\mathrm{T}}$, $\boldsymbol{\Xi}_{515} = -\bar{h}\boldsymbol{e}^{\alpha_2\tau(t)}\bar{\boldsymbol{K}}^{\mathrm{T}}$, $\boldsymbol{\Xi}_{66} = -\gamma_2^2\boldsymbol{I}$,
$\boldsymbol{\Xi}_{612} = -\bar{h}\boldsymbol{e}^{\alpha_2\tau(t)}\bar{\boldsymbol{K}}^{\mathrm{T}}$, $\boldsymbol{\Xi}_{613} = -\sqrt{\bar{h}}\,\boldsymbol{e}^{\alpha_2\tau(t)}\bar{\boldsymbol{K}}^{\mathrm{T}}$,
$\boldsymbol{\Xi}_{614} = -\bar{h}^{\frac{3}{2}}\boldsymbol{e}^{\alpha_2\tau(t)}\bar{\boldsymbol{K}}^{\mathrm{T}}$, $\boldsymbol{\Xi}_{615} = -\bar{h}\boldsymbol{e}^{\alpha_2\tau(t)}\bar{\boldsymbol{K}}^{\mathrm{T}}$,
$\boldsymbol{\Xi}_{77} = -\gamma_2^2\boldsymbol{I}$, $\boldsymbol{\Xi}_{712} = -\bar{h}\boldsymbol{e}^{\alpha_2\tau(t)}\boldsymbol{E}_f^{\mathrm{T}}\bar{\boldsymbol{P}}$,
$\boldsymbol{\Xi}_{713} = -\sqrt{\bar{h}}\,\boldsymbol{e}^{\alpha_2\tau(t)}\boldsymbol{E}_f^{\mathrm{T}}\bar{\boldsymbol{P}}$, $\boldsymbol{\Xi}_{714} = -\bar{h}^{\frac{3}{2}}\boldsymbol{e}^{\alpha_2\tau(t)}\boldsymbol{E}_f^{\mathrm{T}}\bar{\boldsymbol{P}}$,
$\boldsymbol{\Xi}_{715} = -\bar{h}\boldsymbol{e}^{\alpha_2\tau(t)}\boldsymbol{E}_f^{\mathrm{T}}\bar{\boldsymbol{P}}$, $\boldsymbol{\Xi}_{88} = -\gamma_2^2\boldsymbol{I}$, $\boldsymbol{\Xi}_{812} = \bar{h}\boldsymbol{E}_w^{\mathrm{T}}\bar{\boldsymbol{P}}$,
$\boldsymbol{\Xi}_{813} = \sqrt{\bar{h}}\,\boldsymbol{E}_w^{\mathrm{T}}\bar{\boldsymbol{P}}$, $\boldsymbol{\Xi}_{814} = \bar{h}^{\frac{3}{2}}\boldsymbol{E}_w^{\mathrm{T}}\bar{\boldsymbol{P}}$, $\boldsymbol{\Xi}_{815} = \bar{h}\boldsymbol{E}_w^{\mathrm{T}}\bar{\boldsymbol{P}}$,
$\boldsymbol{\Xi}_{99} = -\sigma\boldsymbol{\Phi}$, $\boldsymbol{\Xi}_{1010} = \boldsymbol{\Phi}$, $\boldsymbol{\Xi}_{1111} = \dfrac{1}{-9h}\bar{\boldsymbol{Z}}^{-1}$,
$\boldsymbol{\Xi}_{1212} = -\bar{\boldsymbol{P}}\bar{\boldsymbol{R}}^{-1}\bar{\boldsymbol{P}}$, $\boldsymbol{\Xi}_{1313} = -\bar{\boldsymbol{P}}\bar{\boldsymbol{Z}}^{-1}\bar{\boldsymbol{P}}$, $\boldsymbol{\Xi}_{1414} = -\bar{\boldsymbol{P}}\boldsymbol{Q}_3^{-1}\bar{\boldsymbol{P}}$,
$\boldsymbol{\Xi}_{1515} = -\bar{\boldsymbol{P}}\boldsymbol{Q}_5^{-1}\bar{\boldsymbol{P}}$.

The proof and solution of **Theorem 2** are similar to **Theorem 1**, and will not be repeated here.

5 Simulation experiment and result analysis

5.1 Simulation examples and related parameter settings

In order to verify the feasibility and effectiveness of the proposed method, the four-capacity water tank model is used to complete the simulation experiment[24]. The model parameters are

$$\boldsymbol{A} = \begin{bmatrix} -0.016 & 0 & 0.042 & 0 \\ 0 & -0.011 & 0 & 0.033 \\ 0 & 0 & -0.042 & 0 \\ 0 & 0 & 0 & -0.033 \end{bmatrix},$$

$$\boldsymbol{B} = \begin{bmatrix} 0.083 & 0 \\ 0 & 0.063 \\ 0 & 0.048 \\ 0.031 & 0 \end{bmatrix}, \boldsymbol{B}_w = \begin{bmatrix} 0.01 \\ 0.01 \\ 0 \\ 0.01 \end{bmatrix}, \boldsymbol{E}_v = \begin{bmatrix} 0.01 \\ 0 \\ 0.01 \\ 0.01 \end{bmatrix},$$

$$\boldsymbol{C} = 0.5\boldsymbol{I}_4, \boldsymbol{E}_f = -\begin{bmatrix} 0.083 & 0 & 0 & 0.031 \end{bmatrix}^{\mathrm{T}}.$$

Take the sampling period $h = 0.1$ s, and the simulation time is 800 s. Considering the randomness of DoS attacks, Fig. 3 shows the sequence diagram of blocking the communication interval when limited energy DoS attacks occurs, so that it occurs between 150 s and 800 s. Among them, in 150 s $\leqslant t <$ 500 s, it is small-energy DoS attacks, and in 500 s $\leqslant t \leqslant$ 800 s, it is large-energy DoS attacks. The solid line indicates the blocking communication interval, that is, the data packet cannot be sent normally in this interval.

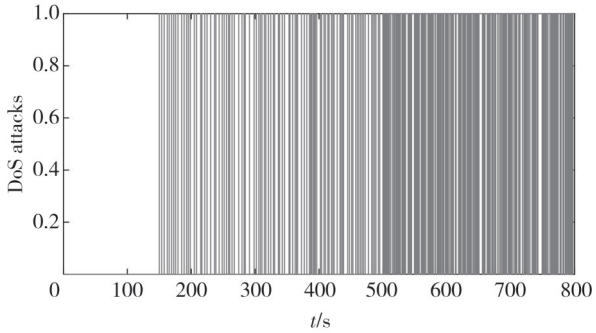

Fig. 3 DoS attacks energy sequence diagram

Continuous time-varying faults are[16]

$$f(t) = \begin{cases} 0, & t \leqslant 250 \text{ s}, \\ 2 + 2\sin 0.01\pi(t - 250), & 250 \text{ s} < t \leqslant 800 \text{ s}. \end{cases}$$

The actuator failure occurs between 250 s and 800 s,

x_1, x_2, x_3, x_4 represent the water level change of the four-capacity water tank, and y_1, y_2, y_3, y_4 represent the observed value of the corresponding water level change. At the same time, two pumps are used to supply water to the four-capacity water tank, and the control input of the water pump is $\boldsymbol{u}(t)$. Assuming that there are disturbance $\boldsymbol{w}(t)$ and noise $\boldsymbol{v}(i_k)$ of the Gaussian white noise process subject to $N(0.1, 0.01)$ in the simulation process, the initial state is $\boldsymbol{x}(0)=[4 \quad 4 \quad 2 \quad 2]^{\mathrm{T}}$.

5.2 State and fault estimation under multi-objective constraints

For the state and fault estimation observer designed in this paper, $\alpha_1=0.05$, $\gamma_1=5$, $\beta=0.8$, $\bar{h}=0.5$ are given. Among them, $\alpha_1=0.05$ is the stability constraint parameter of α-, whose value represents that the closed-loop poles of the system are all located at the left side of -0.05 on the left half plane of S plane. $\gamma_1=5$ is a parameter of disturbance rejection rate. The smaller the value, the stronger the system's ability to suppress disturbance. $\beta=0.8$ is the safety factor, that is, the parameter affecting the intersection of the passive intrusion tolerance area and the active intrusion tolerance area of the DoS attack. $\bar{h}=0.5$ is the graded detection time threshold of passive intrusion tolerance and active intrusion tolerance, that is, the maximum allowable delay of the system exceeds 0.5 s, and the active intrusion tolerance method is adopted, otherwise the passive intrusion tolerance method is adopted.

According to **Theorem 1**, the observer gain matrix $\boldsymbol{L}$ and the fault estimation gain matrix $\boldsymbol{F}$ are

$$\boldsymbol{L}=\begin{bmatrix} 0.850\,2 & -1.553\,7 & -0.661\,2 & 1.621\,3 \\ 0.024\,5 & 0.944\,7 & 0.016\,8 & -0.005\,2 \\ -0.016\,6 & -0.010\,3 & 0.577\,0 & 0.053\,2 \\ 0.023\,2 & -0.593\,6 & -0.232\,7 & 1.355\,7 \end{bmatrix},$$

$$\boldsymbol{F}=[5.208\,6 \quad 31.003\,5 \quad 7.333\,8 \quad -26.829\,3].$$

Figs. 4—6 show the simulation results of state estimation error, actuator fault estimation, and fault estimation error, respectively.

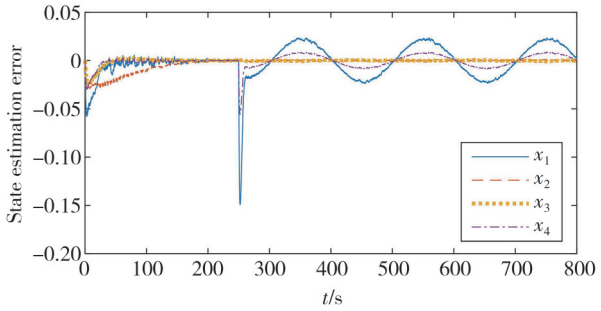

Fig. 4 Diagram of state estimation error

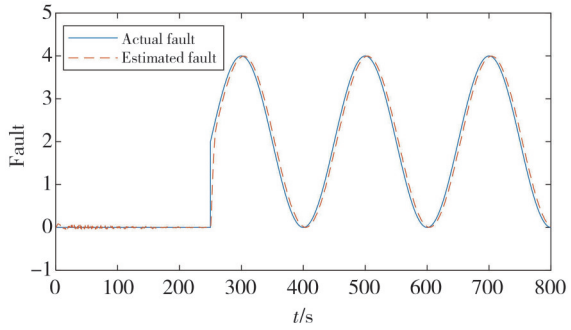

Fig. 5 Actual and estimated faults of actuator

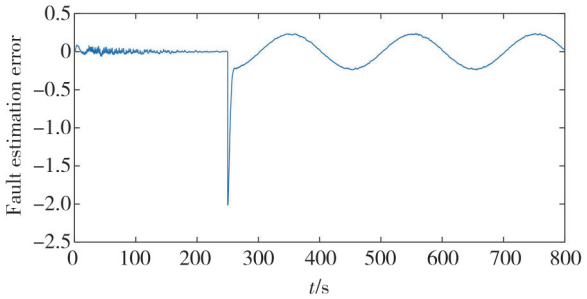

Fig. 6 Diagram of fault estimation error

It can be seen that at $t \leqslant 150$ s, the system has no faults and no attacks, and only external disturbances exist, and the state estimation error and fault estimation error of the system both tend to be 0. It can be seen that the observer has the ability to suppress external ability to disturb. At 150 s $< t \leqslant$ 250 s, the system has no faults, but there are small-energy DoS attacks. It can be seen that under the action of system "elasticity", the error between the state and fault estimation of the system still remains near 0. At 250 s $< t \leqslant$ 500 s, when the actuator fault is applied, the error between the initial state and the fault estimation is large, but it quickly converges to near 0, the state estimation error keeps fluctuating between ± 0.03, and the fault estimation error remains between ± 0.25 fluctuation. At 500 s $< t \leqslant$ 800 s, when the fault and external disturbance remain unchanged, the DoS attacks energy is increased, and the active-passive hybrid intrusion tolerance strategy is adopted. It can be seen that the state and fault estimation of the system is basically unaffected.

To sum up, the state and fault estimation observer can accurately estimate the system state and fault information for ICPS with coexistence of DoS attacks of different energy levels and actuator failure, and lay a foundation for the design of comprehensive security control devices.

5.3 Comprehensive security control under multi-objective constraints

For the designed integrated safety controller,

according to $(\boldsymbol{I}-\boldsymbol{B}\boldsymbol{B}^{+})\boldsymbol{E}_f=\boldsymbol{0}$, the fault adjustment matrix can be obtained by

$$\boldsymbol{B}^{+}=\begin{bmatrix}11.955\,0 & -10.573\,2 & 0 & 0.249\,6\\ 0 & 0 & 0 & 0\end{bmatrix}.$$

Given the parameter values $\gamma_2=4$, $\sigma=0.001$, $\alpha_2=0.04$, the event trigger weight matrix $\boldsymbol{\Phi}$ and the state feedback gain matrix $\boldsymbol{K}$ can be obtained by **Theorem 2**, i.e.,

$$\boldsymbol{\Phi}=10^{-8}\times\begin{bmatrix}0.146\,3 & 0 & 0 & 0\\ 0 & 0.146\,3 & 0 & 0\\ 0 & 0 & 0.146\,3 & 0\\ 0 & 0 & 0 & 0.146\,3\end{bmatrix},$$

$$\boldsymbol{K}=\begin{bmatrix}-0.282\,5 & 0.452\,6 & -0.146\,0 & -1.513\,0\\ 0.028\,1 & -0.011\,7 & -0.546\,5 & -0.152\,6\end{bmatrix}.$$

Fig.7 shows the output response curves of the system with attack active and passive hybrid intrusion tolerance and fault active fault tolerance.

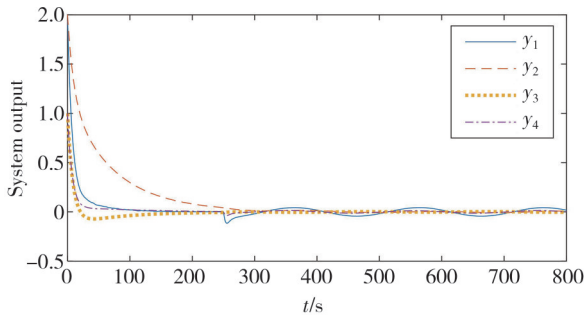

Fig. 7 Response curves of system output

It can be seen that in the case of adding the DoS attacks and the failure mode as mentioned above, except at the moment of adding the failure, the output response curve of the system fluctuates slightly, but under the action of the comprehensive safety controller, the equilibrium state is quickly restored. And whether it is under small-energy DoS attacks or large-energy DoS attacks, under the active and passive intrusion tolerance strategy, the system output response curve is basically not affected by the attack, and can still tend to a balanced state.

Fig. 8 shows the prediction and compensation measurement data under the high-energy DoS attacks after 500 s. It can be seen that the prediction data almost coincides with the real data by using the proposed time series analysis prediction compensation method. In order to further reflect the accuracy of the compensation data, Fig.9 shows the error between the compensation data and the real data after 500 s, and the compensation error is kept within a small range, which ensures the reliability of the prediction data.

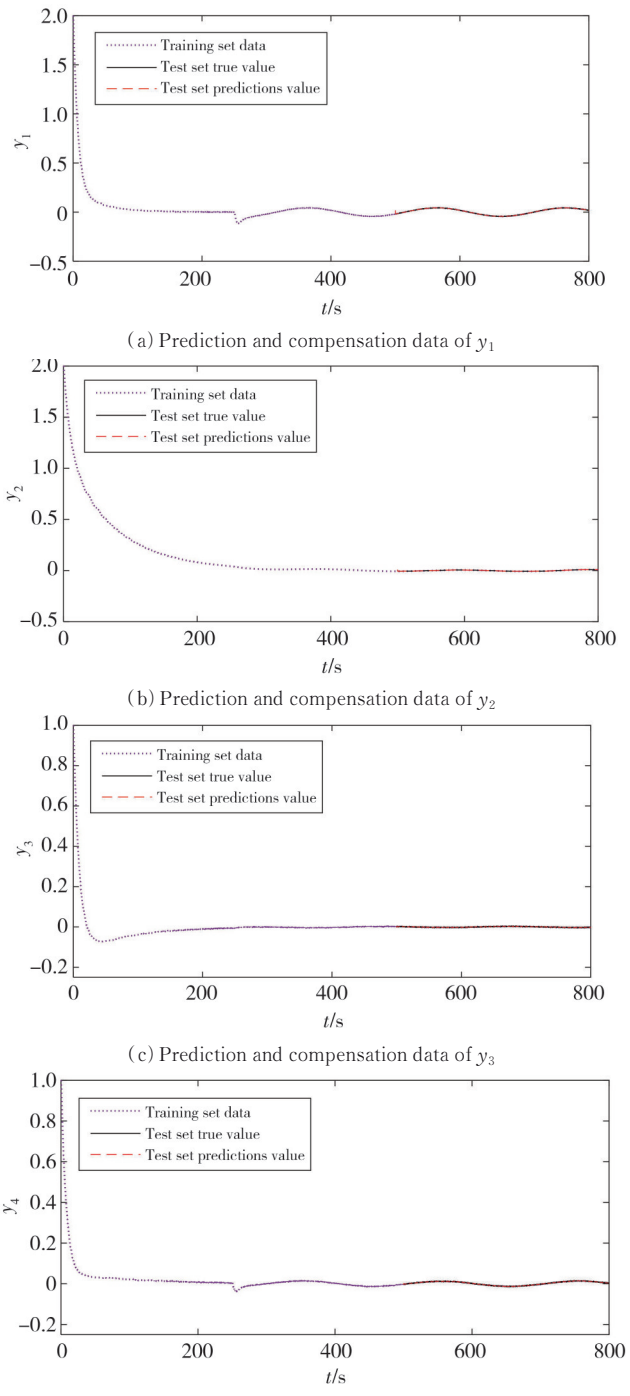

(a) Prediction and compensation data of y_1

(b) Prediction and compensation data of y_2

(c) Prediction and compensation data of y_3

(d) Prediction and compensation data of y_4

Fig. 8 Prediction and compensation data under high power DoS attacks

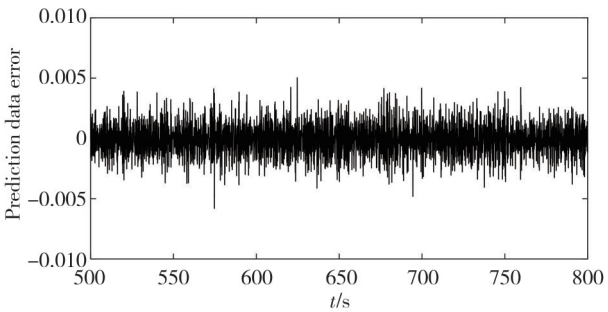

Fig. 9 Prediction data compensates for errors

In order to further highlight the effectiveness of the active compensation strategy, under the condition that the attack and fault remain unchanged, Fig.10 shows the system output response curve of the passive intrusion tolerance method only for the limited energy DoS attacks. It can be seen from the simulation results that after adding a high-energy DoS attacks at $t=500$ s, the fluctuation of the system output response curve increases significantly. Obviously, only passive intrusion tolerance methods cannot effectively defend against large-energy DoS attacks. It shows that the active-passive hybrid intrusion tolerance method is effective for the defense against large DoS attacks.

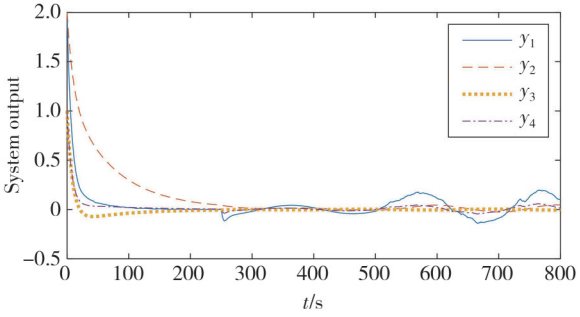

Fig. 10 Output response curves of system under dynamic intrusion

α_2 as a key parameter affecting the dynamic performance of the system, the increase of its value means further improvement of the system performance. Under the premise of limiting $\gamma_2=4$, $\sigma=0.001$, Table 1 shows the average data packet transmission period, data packet transmission rate, and the change of the number of control unit calculations under different α_2.

Table 1 Influence of different α_2 parameters on communication and computing resources

α_2	h_{av}/s	η/%	m
0	0.225	31.2	3 555
0.02	0.202	35.8	3 960
0.04	0.184	40.5	4 347
0.06	0.165	46.1	4 848

h_{av} is the average transmission period of data packets, η is the transmission rate of data packets, indicating the ratio of triggered and successfully transmitted data packets under DETCS to the cycle time trigger mechanism, and m is the number of calculations by the control unit.

It can be seen from Table 1 that with the increase of α_2, the average data packet transmission period gradually decreases, but the data packet transmission rate and calculation amount gradually increase. So the improvement of system performance is at the cost of sacrificing communication resources and computing resources. Therefore, in actual engineering, we cannot blindly increase α_2 to improve system performance. We should weigh the pros and cons of system performance, communication resources, and computing resources according to the network environment where the system is located and the possible DoS attacks situation. Then more reasonable parameters are selected to achieve the optimal goal of comprehensive security control.

Considering the randomness of DoS attacks time, under the premise of limiting $\gamma_2=4$, $\sigma=0.001$, Table 2 shows the impact of different triggering intervals $\bar{h}$ on the system under multiple simulation studies. The physical meanings of h_{av} and m are the same as those in Table 1. ρ is the calculation rate.

Table 2 Effects of different trigger time intervals on system

$\bar{h}$	$h_{av/S}$	ρ/%	m
0.2	0.122	50.26	4 021
0.3	0.135	46.80	3 744
0.4	0.164	42.81	3 425
0.5	0.205	37.18	2 974
0.6	0.237	32.76	2 621

It can be seen from Table 2 that the increase of $\bar{h}$ is accompanied by the increase of h_{av} and the decrease of m, which means that the detection threshold of attack classification increases, the system security and performance are reduced, but the system computing burden is reduced, and certain computing resources are saved. It can be seen that the security and performance of the system and the occupation of computing resources are mutually restricted. In specific practice, reasonable $\bar{h}$ parameters should be selected according to the actual control objectives, which can save computing resources on the basis of ensuring the good security and performance of the system. At the same time, the introduction of $\bar{h}$ also makes the hierarchical detection of attacks more flexible.

6 Conclusions

The collaborative design of ICPS integrated security control and communication under multi-objective constraints was studied, combined with the maximum security trigger interval, a DoS attacks energy classification detection mechanism was designed, and a DoS attacks active and passive hybrid intrusion tolerance strategy was proposed. And the prediction method based on time series analysis was used to effectively compensate for the lost data, and the ICPS comprehensive security control and communication collaborative design method under the multi-objective constraints was given. The simulation experiment was

carried out on a common industrial four-capacity water tank system. The results showed that the proposed method could effectively distinguish and defend against DoS attacks of different energy levels. It could achieve the goal of attack active and passive mixed intrusion tolerance and fault active fault tolerance. Multi-objective constraints enabled the system to effectively suppress the influence of disturbance and noise and have better dynamic performance, which improved the security control level of the system.

Due to different network layouts, when DoS attacks occur on both ends of the system at the same time, how to find a security control strategy for ICPS based on the active-passive hybrid intrusion tolerance idea of DoS energy classification will be a hot spot in the future.

Acknowledgement

This work was supported by Gansu Higher Education Innovation Fund Project (No.2023B-439).

Declaration of conflicting interests

The authors have no conflict of interests related to this publication.

References

[1] AKKAYA I, DERLER P, EMOTO S, et al. Systems engineering for industrial cyber-physical systems using aspects. Proceedings of the IEEE, 2016, 104(5): 997-1012.

[2] KAYAN H K, NUNES M, RANA O, et al. Cybersecurity of industrial cyber-physical systems: a review. 2021: 2101.03564. http://arxiv. org/abs/2101.03564v1.

[3] SHEN Y B. Network security analyzing of event-triggered networked control systems under denial-of-service attacks//The 2nd International Conference on Robotics, Control and Automation Engineering, November 16-18, 2019, Lanzhou, China. New York: ACM, 2019: 49-54.

[4] YE D, ZHANG T Y. Summation detector for false data-injection attack in cyber-physical systems. IEEE Transactions on Cybernetics, 2020, 50(6): 2338-2345.

[5] CHEN B, HO D W C, HU G Q, et al. Secure fusion estimation for bandwidth constrained cyber-physical systems under replay attacks. IEEE Transactions on Cybernetics, 2018, 48(6): 1862-1876.

[6] GONG J H, HU X H, HONG P. Behavior analysis of malicious sensor nodes based on optimal response dynamics. Journal of Measurement Science and Instrumentation, 2022, 13(1): 96-104. .

[7] PENG Y, WANG Y, XIANG C, et al. Cyber-physical attack-oriented industrial control systems (ICS) modeling, analysis and experiment environment//2015 International Conference on Intelligent Information Hiding and Multimedia Signal Processing (IIH-MSP), September 23-25, 2015, Adelaide, SA, Australia. New York: IEEE, 2015: 322-326.

[8] YLMAZ E N, CIYLAN B, GÖNEN S, et al. Cyber security in industrial control systems: Analysis of DoS attacks against PLCs and the insider effect//2018 6th International Istanbul Smart Grids and Cities Congress and Fair (ICSG), April 25-26, 2018, Istanbul, Turkey. New York: IEEE, 2018: 81-85.

[9] FENG S, TESI P. Resilient control under Denial-of-Service: Robust design. Automatica, 2017, 79: 42-51.

[10] ZHANG C L, YANG G H, LU A Y. Resilient observer-based control for cyber-physical systems under denial-of-service attacks. Information Sciences, 2021, 545: 102-117.

[11] GAN R M, XIAO Y, SHAO J L, et al. An analysis on optimal attack schedule based on channel hopping scheme in cyber-physical systems. IEEE Transactions on Cybernetics, 2021, 51(2): 994-1003.

[12] QIN J H, LI M L, WANG J, et al. Optimal Denial-of-Service attack energy management against state estimation over an SINR-based network. Automatica, 2020, 119: 109090.

[13] SONG H T, PENG C, WANG Z W. Event-triggered predictive control for cyber-physical systems under DoS attackss. Control and Decision, 2019, 34(11): 2303-2309.

[14] YE D, DIAO N N, ZHAO X G. Fault-tolerant controller design for general polynomial-fuzzy-model-based systems. IEEE Transactions on Fuzzy Systems, 2018, 26(2): 1046-1051.

[15] ZHANG J X, YANG G H. Fault-tolerant output-constrained control of unknown Euler-Lagrange systems with prescribed tracking accuracy. Automatica, 2020, 111: 108606.

[16] QIU A B, JI H G, GU J P. Optimal integrated design of time-varying fault estimation and accommodation for nonuniformly sampled data systems. Acta Automatica Sinica, 2014, 40(7): 1493-1504.

[17] YE D, CHEN M M, YANG H J. Distributed adaptive event-triggered fault-tolerant consensus of multiagent systems with general linear dynamics. IEEE Transactions on Cybernetics, 2019, 49(3): 757-767.

[18] WANG X D, FEI Z Y, WANG Z H, et al. Event-triggered fault estimation and fault-tolerant control for networked control systems. Journal of the Franklin Institute, 2019, 356(8): 4420-4441.

[19] DENG C, CHE W W. Fault-tolerant fuzzy formation control for a class of nonlinear multiagent systems under directed and switching topology. IEEE Transactions on Systems, Man, and Cybernetics: Systems, 2021, 51(9): 5456-5465.

[20] SHAO X F, YE D. Fuzzy adaptive event-triggered secure control for stochastic nonlinear high-order MASs subject to DoS attacks and actuator faults. IEEE Transactions on

Fuzzy Systems, 2021, 29(12): 3812-3821.

[21] LI J, YANG Z, MU X W, et al. Passivity-based event-triggered fault tolerant control for nonlinear networked control system with actuator failures and DoS jamming attacks. Journal of the Franklin Institute, 2020, 357(14): 9288-9307.

[22] ZHAO L, LI W. Co-design of dual security control and communication for nonlinear CPS under DoS attack. IEEE Access, 2020, 8: 19271-19285.

[23] FRIDMAN E. A refined input delay approach to sampled-data control. Automatica, 2010, 46(2): 421-427.

[24] QIU A B, JIANG B, WEN C L, et al. Fault estimation and accommodation for networked control systems with nonuniform sampling periods. International Journal of Adaptive Control and Signal Processing, 2015, 29(4): 427-442.

DoS攻击能量分级检测与补偿下的ICPS多目标约束综合安全控制

韩寅龙[1], 韩小武[2*]

1. 酒泉职业技术学院 新能源工程学院, 甘肃 酒泉 735000;
2. 西安明德理工学院 智能制造与控制技术学院, 陕西 西安 710124

摘　要: 针对DoS攻击与执行器故障共存的工业信息物理融合系统(Industry cyber-physical system, ICPS), 本文研究了多目标约束下的ICPS综合安全控制问题。首先, 从防御者的角度, 依据系统遭受不同能量DoS攻击所表现的差异化影响, 制定了DoS攻击能量分级标准, 构建了ICPS综合安全控制架构。其次, 设计了基于事件触发的安全传输策略, 在DoS攻击能量分级检测机制下, 针对大能量攻击考虑基于时间序列分析的方法对丢失数据进行预测补偿, 从而在被动弹性应对小能量攻击的基础上增加了对DoS攻击的主动防御能力。接着, 引入锥补线性化算法, 推证出了状态与故障估计观测器、综合安全控制器的求取方法, 实现了DoS攻击主被动混合容侵与执行器故障主动容错的目标。最后, 给出了四容水箱系统仿真示例, 验证了所得结论的有效性。

关键词: 工业信息物理融合系统; DoS攻击能量分级; 安全事件触发机制; 时间序列分析方法; 锥补线性化

引用格式: HAN Yinlong, HAN Xiaowu. ICPS multi-target constrained comprehensive security control based on DoS attacks energy grading detection and compensation. Journal of Measurement Science and Instrumentation, 2024, 15(4): 518-531.